1981

Saturation moments of Gd alloys

John Harold Queen
Iowa State University

INFORMATION TO USERS

This was produced from a copy of a document sent to us for microfilming. While the most advanced technological means to photograph and reproduce this document have been used, the quality is heavily dependent upon the quality of the material submitted.

The following explanation of techniques is provided to help you understand markings or notations which may appear on this reproduction.

1. The sign or "target" for pages apparently lacking from the document photographed is "Missing Page(s)". If it was possible to obtain the missing page(s) or section, they are spliced into the film along with adjacent pages. This may have necessitated cutting through an image and duplicating adjacent pages to assure you of complete continuity.

2. When an image on the film is obliterated with a round black mark it is an indication that the film inspector noticed either blurred copy because of movement during exposure, or duplicate copy. Unless we meant to delete copyrighted materials that should not have been filmed, you will find a good image of the page in the adjacent frame. If copyrighted materials were deleted you will find a target note listing the pages in the adjacent frame.

3. When a map, drawing or chart, etc., is part of the material being photographed the photographer has followed a definite method in "sectioning" the material. It is customary to begin filming at the upper left hand corner of a large sheet and to continue from left to right in equal sections with small overlaps. If necessary, sectioning is continued again—beginning below the first row and continuing on until complete.

4. For any illustrations that cannot be reproduced satisfactorily by xerography, photographic prints can be purchased at additional cost and tipped into your xerographic copy. Requests can be made to our Dissertations Customer Services Department.

5. Some pages in any document may have indistinct print. In all cases we have filmed the best available copy.

University
Microfilms
International

300 N. ZEEB RD., ANN ARBOR, MI 48106

Queen, John Harold

SATURATION MOMENTS OF GADOLINIUM ALLOYS

Iowa State University PH.D. 1981

Saturation moments of Gd alloys

by

John Harold Queen

A Dissertation Submitted to the

Graduate Faculty in Partial Fulfillment of the

Requirements for the Degree of

DOCTOR OF PHILOSOPHY

Department: Physics
Major: Solid State Physics

Approved:

Signature was redacted for privacy.

In Charge of Major Work

Signature was redacted for privacy.

For the Major Department

Signature was redacted for privacy.

For the Graduate College

Iowa State University
Ames, Iowa

1981

TABLE OF CONTENTS

I. INTRODUCTION

In the study of magnetism and magnetic phenomena, the rare earth or lanthanide metals hold a unique place among the elements. The large variety of intricate magnetic properties displayed by the rare earths is a result of their electronic configuration. This configuration may be written schematically as follows:

$$(Xe)(4f)^{n}(5d)^{1}(6s)^{2}$$

where n, the number of 4f electrons, varies across the series from zero for lanthanum to 14 for lutetium. The crystalline structures of most of the rare earth metals are similar, consisting of triply ionized atoms such that the gross chemical and physical properties are nearly identical. The interesting magnetic properties are due to the highly localized, highly screened, unpaired 4f electrons.

The ground state configuration of the 4f electrons is given by the Hund rules. Under the Hund rules, the ground state of a given shell of an atom is characterized by the following:

The maximum value of the total spin S allowed by the exclusion principle;

The maximum value of the orbital angular momentum L consistent with this value of S; and

The value of the total angular momentum J is equal to $|L - S|$ for less than half filled shells, and equal to $L + S$ for more than half filled shells. For a half filled shell, $J = S$.

As will be discussed further in the theory section, a magnetic moment is associated with the total angular momentum J resulting from the unpaired 4f electrons.

Because of the highly localized nature of the 4f electrons and their associated moments, a direct Heisenberg exchange mechanism is insufficient in accounting for the ordering of moments observed in the rare earths. Rather, it is believed that an indirect exchange coupling mediated by the conduction electrons is responsible for the intricate magnetic ordering schemes observed in the rare earths. Details of this interaction will be discussed in the theory section, but it is appropriate to present some of the results at this time.

A primary result of the indirect exchange mechanism is that the coupling between two neighboring rare earth ions may be viewed as an effective direct exchange coupling proportional to the dot product of the two spins. That is,

$$E_{ex} \propto \bar{S}_1 \cdot \bar{S}_2 \tag{1}$$

where $\bar{S}_1$ and $\bar{S}_2$ are the spin vectors associated with neighboring ions 1 and 2. Because of spin-orbit coupling, the spin vector of a rare earth ion will precess about the J vector. For this reason, it was suggested by De Gennes that the projection of the spin vector onto the J vector, and not the spin vector itself, should appear in the exchange energy. That is,

$$E_{ex} \propto (g - 1)^2 \bar{J}_1 \cdot \bar{J}_2 \tag{2}$$

where $(g - 1)\bar{J}$ is the projection of $\bar{S}$ onto $\bar{J}$.

The validity of this suggestion has been the basis of a great deal of experimental work in the past, and is indeed the basic question to which the present work is addressed. One result of the indirect exchange coupling which immediately lends itself to experimental investigation in regard to the validity of the suggestion of de Gennes is the prediction of the initial ordering temperatures. Assuming that the exchange matrix element is constant across the rare earth series, the indirect exchange interaction predicts that the initial ordering temperatures should be proportional to either $S(S + 1)$ or, if the suggestion of de Gennes is valid, $(g - 1)^2J(J + 1)$. Legvold (1) has recently pointed out that the highest observed initial ordering temperatures of the rare earths, as well as the average paramagnetic ordering temperatures, are proportional to $S(S + 1)$ and not $(g - 1)^2J(J + 1)$. However, he points out the fact that this result may be coincidental due to the possibility that the exchange constant may vary across the rare earth series.

Another manifestation of the nature of the exchange interaction is the spin disorder resistivity. As is further discussed in the theory section, if the suggestion of de Gennes is valid, the spin disorder resistivity should be proportional to $(g - 1)^2J(J + 1)$. Calculations of the spin disorder resistivity based on raw data corrected for phonon and impurity scattering in the heavy rare earth metals have been reported by Anderson and Legvold (2). They found that the spin disorder resistivity was proportional to $S(S + 1)$ and not $(g - 1)^2J(J + 1)$. Brout and Suhl (3) deemed these results as "quite likely to be quantitatively unreliable"

due to the subtraction process involved. More recent measurements of the electrical resistivities of rare earth single crystals have been analyzed by Legvold (4). He found that, without corrections for Fermi-surface effect, the total spin disorder resistivity of heavy rare earth single crystals was proportional to $S(S + 1)$ in the basal plane and to $(g - 1)^2 J(J + 1)$ in the c-direction. After Fermi-surface effects were included, his results indicated a $(g - 1)^2 J(J + 1)$ dependence in both directions. Mackintosh and Smidt (5) performed electrical resistivity measurements on dilute alloys of heavy rare earths in lutetium and found that the spin disorder contribution was proportional to $(g - 1)^2 J(J + 1)$. While attempting to reproduce these results in dilute alloys of heavy rare earths in thorium, Legvold et al. (6) found that Coulomb scattering is an important effect. After adjusting the data of Mackintosh and Smidt for the dependence on atomic volume, an $S(S + 1)$ dependence was found.

Thus, it has been seen that the experimental results to date are inconclusive at best, and that no definitive experiment testing the de Gennes suggestion has been reported. One further area in which the suggestion of de Gennes should be manifest is the saturation magnetization of ferromagnetic rare earth alloys. In such alloys, the net magnetic moment will be determined by the relative orientations of the J vectors of the two constituents. Since there is some finite angle between $\bar{J}$ and $\bar{S}$, the expected saturation magnetizations will differ, depending on whether S-S coupling or J-J coupling is appropriate. For J-J coupling, the two J vectors of the constituents will be in parallel or antiparallel

alignment in the ground state. The corresponding magnetic moment in this case will be either the sum or difference of the moments of the constituents. For S-S coupling the spin vectors will agign, but since $\overline{S}$ and $\overline{J}$ are not in the same direction, the moments will no longer be parallel or antiparallel, and a different saturation magnetization is expected. These considerations will be greatly simplified if gadolinium is chosen as one of the constituents, since gadolinium is characterized by a pure spin moment. Thus, it is suggested that measurements of the saturation magnetizations of alloys of light rare earths with gadolinium may shed some light on the validity of the de Gennes proposal.

II. THEORY

A. Elementary Theory of Magnetic Ordering

The highly localized magnetic moment characteristic of most of the rare earth ions is believed to be a direct result of the orbital and spin angular momenta of the unpaired 4f electrons. The magnetic moment arising from the total orbital momentum L combines with the magnetic moment arising from the total spin angular momentum S to yield a total average moment whose component in the direction of applied field is given by

$$M = g\mu_B J \tag{3}$$

where μ_B is the Bohr magneton, given by $\mu_B = 9.2741 \times 10^{-21}$ erg/Oe, and g, the Lande g factor, is given by

$$g = 1 + \frac{J(J+1) - L(L+1) + S(S+1)}{J(J+1)} \quad . \tag{4}$$

At sufficiently high temperatures, any interactions which would tend to bring about an ordered magnetic structure within a rare earth crystal are overshadowed by thermal randomization processes. Thus, at higher temperatures, the rare earth crystal will consist of an arrangement of localized noninteracting magnetic moments. This temperature regime is known as the paramagnetic regime. While there is no spontaneous magnetic moment associated with the paramagnetic regime, the system will have a response to an applied field. Calculations based on quantum mechanics and statistical mechanics lead to the result that the net magnetization per gram of a paramagnetic solid is given by

$$\sigma = \frac{N_0 g \mu_B J B_J(x)}{A} \tag{5}$$

where $x = gJ\mu_B H/kT$, T is the temperature, k is the Boltzman constant, N_0 is Avogadro's number, A is the atomic weight, and $B_J(x)$ is the well-known Brillouin function. In the low field or high temperature limit, Eq. 5 becomes

$$\sigma = \frac{N_0 J(J+1) g^2 \mu_B^2}{3kAT} H \tag{6}$$

which is the famous Curie law for the response of a paramagnetic system to an applied field as a function of temperature.

Certain magnetic ions, when arrayed in a lattice, interact by mechanisms that will be detailed in later discussion. Below certain temperatures, these interactions between the various moments may be strong enough to overcome the thermal randomization processes and thus bring about a long range order to the magnetic moments of the crystal. The exact nature of this ordering is strongly dependent on the details of the interaction, and indeed some very sophisticated and complex ordering schemes have been observed in the rare earths. As an example of one of the simpler cases of magnetic ordering, the case of simple ferromagnetic ordering will be examined.

A simple ferromagnet consists of a system of interacting magnetic moments all aligned parallel to each other. The simple ferromagnet was first treated phenomenologically by Weiss (7). Weiss observed that in zero applied magnetic field, a ferromagnet still exhibits a spontaneous moment. This fact was taken to indicate that an additional internal

magnetic field must exist within the ferromagnet. Weiss treated this field by the introduction of a molecular field H_m, which is proportional to the net magnetic moment of the system. Thus, the total field present in the material is the sum of the applied field H and the molecular field H_m. Thus,

$$H_t = H + H_m = H + W\sigma \tag{7}$$

where σ is the moment per gram, and W is an interaction constant, incorporating the interactions between the moments into an equivalent interaction between a single moment and the average interaction with all of its neighbors. This total field is then placed into Eq. 5 by the substitution $x = g\mu_B J(H + W\sigma)/kT$. After this substitution has been made, the low field or high temperature limit becomes

$$\sigma = \frac{C}{T - \theta_p} H \tag{8}$$

which is the well-known Curie-Weiss law, where $\theta_p = WC$, and where C, the Curie constant, is given by

$$C = \frac{N_0 J(J + 1) g^2 \mu_B^2}{3kA} . \tag{9}$$

It is an experimental fact that the magnetization of many ferromagnetic materials is very well-described by Eq. 7.

The primary quantity of interest in the problem under consideration is the saturation magnetization. The saturation magnetization is the magnetization which would be attained in an infinite field with all the magnetic moments aligned. Saturation magnetization is usually measured

in units of emu/gm. This quantity may be converted into moment per atom by the conversion relation

$$\mu_{sat} = \frac{A\sigma_{\infty,0}}{5585} \mu_B \tag{10}$$

where $\sigma_{\infty,0}$ is the saturation magnetization in emu/gm. The saturation moment per atom is given by Eq. 3.

B. Indirect Exchange

In order to understand any further details of the ferromagnetically ordered state, it is necessary to examine the interactions between the various ions in further detail. These interactions give rise to the molecular field, and they will be directly related to the constant W of the molecular field approximation.

The basic mechanism leading to these interactions is exchange. Heisenberg (8) showed that ferromagnetism could be accounted for by the exchange interactions between neighboring ions. The interaction Hamiltonian is given by

$$H = -2 \sum_{i,j} J_{ij} \bar{S}_i \cdot \bar{S}_j \tag{11}$$

where J_{ij} is the exchange integral between the electron wave functions of ions i and j, and $\bar{S}_i$ and $\bar{S}_j$ are the spins of ions i and j, respectively. In certain materials, the direct Heisenberg exchange process is believed to be the dominant interaction leading to magnetic ordering. In the case of the rare earths, however, the highly localized spins are associated with the 4f electrons. The overlap of 4f electron wave

functions between neighboring ions is not large enough to produce significant exchange, and the direct exchange integral J_{ij} is essentially zero. Thus, the direct exchange mechanism of Heisenberg does not account for magnetic ordering observed in the rare earths.

The failure of a direct exchange process to account for magnetic ordering in the rare earths brought about a need for a more complicated theory. Ruderman and Kittel (9) proposed an indirect exchange mechanism to explain certain nuclear hyperfine splittings. Their ideas were extended to the case of coupling between localized magnetic moments by Kasuya (10) and Yosida (11). In the RKKY model, as it has come to be known, a conduction electron interacts through a direct exchange mechanism with an ion of spin $\overline{S}_i$ at $\overline{R}_i$. The conduction electron then interacts via a direct exchange mechanism with a neighboring ion with spin $\overline{S}_j$ at $\overline{R}_j$. When the electron interacts with the ion at $\overline{R}_j$, its initial state has been determined by its previous interaction with the ion at $\overline{R}_i$. Thus, the conduction electrons carry information about the state of the ion at $\overline{R}_i$ to the ion at $\overline{R}_j$. This process also leaves the conduction electrons with a net spin polarization.

This indirect exchange mechanism will now be considered in further detail. The interaction between an ion of spin $\overline{S}_j$ at $\overline{R}_j$ and a conduction electron of spin $\overline{\sigma}_i$ at $\overline{r}_i$ is given by the Hamiltonian

$$H_{int} = -I(\overline{r}_i - \overline{R}_j)\overline{\sigma}_i \cdot \overline{S}_j \ . \qquad (12)$$

In general, the interaction Hamiltonian should include anisotropic interaction effects. These effects arise from the orbital contribution,

and include anisotropic exchange, crystal field effects, and terms arising from magnetoelastic effects. Fortunately, the essential ordering information can be obtained from Eq. 12, and in the name of simplicity, these effects will be ignored. Another simplifying assumption that is made is that the interaction between the conduction electrons and the 4f electrons is a point interaction. Thus,

$$I(\bar{r}_i - \bar{R}_j) = I\delta(\bar{r}_i - \bar{R}_j) \tag{13}$$

where I is a constant. Following the procedure of Kasuya (12), the Hamiltonian of Eq. 12 is modified by the assumption of Eq. 13 and then second quantized with respect to the conduction electron states to give

$$\begin{aligned} H_{int} = -I \sum_j \sum_{\substack{k,k' \\ s,s'}} [& \langle \psi_{k',s'} | \delta(r - R_j)\sigma^z | \psi_{k,s} \rangle S_j^z \\ & + \frac{1}{2} \langle \psi_{k',s'} | \delta(r - R_j)\sigma^+ | \psi_{k,s} \rangle S_j^- \\ & + \frac{1}{2} \langle \psi_{k',s'} | \delta(r - R_j)\sigma^- | \psi_{k,s} \rangle S_j^+] C_{k',s'}^+ C_{k,s}^- \end{aligned} \tag{14}$$

where $C_{k,s}^+$ and $C_{k,s}^-$ are the usual creation and annihilation operators for conduction electrons of momentum k and spin s. The electron wave functions in the crystal are Bloch states, and are given by

$$\psi_{k,s} = e^{i\bar{k}\cdot\bar{r}} U_k(\bar{r}) g_s \tag{15}$$

where g_s is a spin function. Eq. 15 is then substituted into the Hamiltonian of Eq. 14 to give the result

$$H_{int} = -I/2 \sum_{j} \sum_{k,k'} U^{*}_{k'}(\bar{R}_j)U_k(\bar{R}_j)e^{i(\bar{k}-\bar{k}')\cdot\bar{R}_j}$$

$$[S^z_j(C^+_{k'+}C^-_{k+} - C^+_{k'-}C^-_{k+}) + S^-_j C^+_{k+}C^-_{k'-} + S^+_j C^+_{k'-}C^-_{k+}] \quad . \qquad (16)$$

The interaction Hamiltonian of Eq. 16 is considered as a perturbation term and treated by the usual methods of standard perturbation theory. The first order perturbation term is zero. This is seen from the fact that the first order energy term involves a matrix element between two ground states. The zeroth-order state of the conduction electrons in metals is usually paramagnetic and there is no spin polarization. Hence, the matrix elements will be zero since the terms in the Hamiltonian of Eq. 16 act to flip the spins. Thus, second order perturbation theory must be used. The second order term is

$$E^{(2)} = I^2/4 \sum_{i,j} \sum_{k,k'} [n_k(1 - n_{k'}) U^{*}_{k'}(\bar{R}_j)U_{k'}(\bar{R}_i)U_k(\bar{R}_j)U^{*}_k(\bar{R}_i)]$$

$$\frac{e^{i(\bar{k}-\bar{k}')\cdot(\bar{R}_j-\bar{R}_i)}}{(E_k - E_{k'})} \; 2\bar{S}_i \cdot \bar{S}_j \qquad (17)$$

or equivalently

$$E^{(2)} = -\sum_{i,j} J_{ij}\bar{S}_i \cdot \bar{S}_j$$

$$J_{ij} = -I^2/2 \sum_{k,k'} n_k(1 - n_{k'})[U^{*}_{k'}(\bar{R}_j)U_{k'}(\bar{R}_i)U_k(\bar{R}_j)U^{*}_k(\bar{R}_i)] \qquad (18)$$

$$\frac{e^{i(\bar{k}-\bar{k}')\cdot(\bar{R}_j-\bar{R}_i)}}{(E_k - E_{k'})} \; .$$

Comparison of Eq. 18 with Eq. 11, the Heisenberg expression for direct exchange coupling, shows that the indirect exchange interaction between conduction electrons and the local moments can be viewed as an effective direct exchange coupling of the form

$$E^{(2)} = -\sum_{i,j} J_{ij} \bar{S}_i \cdot \bar{S}_j \ .$$

All the conduction electron information is now contained in the extremely complex exchange constant J_{ij}. In reality, the conduction electron states are distributed over several bands, and there is not a unique electron state for each value of momentum and spin. In order to account for this additional complication, a band index b is introduced. The Hamiltonian describing the interaction then becomes

$$H_{int} = -\sum_{i,j} J_{ij} \bar{S}_i \cdot \bar{S}_j$$

$$J_{ij} = \frac{1}{2} \sum_{\substack{b,k \\ b',k'}} \frac{(n_{b,k} - n_{b',k'}) |< bk \ I_{ex} \ b'k' >|^2 e^{i(\bar{k}-\bar{k}')\cdot\bar{R}_{ij}}}{E_{b,k} - E_{b',k'}} \ . \quad (19)$$

A simplifying assumption which is commonly made is that the exchange matrix element $<I_{ex}>^2$, which is a function of $\bar{k}$ and $\bar{k}'$, can be assumed to be a function of $\bar{k} - \bar{k}' = \bar{q}$. Under this assumption, Eq. 19 reduces to

$$H_{int} = -\sum_{i,j} J_{ij} \bar{S}_i \cdot \bar{S}_j$$

$$J_{ij} = \frac{1}{4} \sum_{\bar{q}} I^2(\bar{q}) \chi(\bar{q}) e^{i\bar{q}\cdot\bar{R}_{ij}} \qquad (20)$$

$$\chi(\bar{q}) = \sum_{\substack{\bar{k} \\ b,b'}} \frac{n_{b,\bar{k}} - n_{b',\bar{k}+\bar{q}}}{E_{b,\bar{k}} - E_{b',\bar{k}+\bar{q}}} .$$

The quantity $\chi(\bar{q})$ is known as the generalized susceptibility. When combined with the exchange matrix element, which is usually assumed to be constant across the rare earths, it contains information on the nature of the expected ordering. The constraints of energy minimization dictate that the localized spins will assume a magnetic structure that has a periodicity corresponding to the maximum in the generalized susceptibility function. The form of the stable magnetic structure is determined by $J(\bar{Q})$ which is defined as the maximum value of $J(\bar{q}) = I^2(\bar{q})\chi(\bar{q})$, where $\bar{Q}$ is the value of $\bar{q}$ giving a maximum in $J(\bar{q})$. Thus, it is seen that the complex ordering schemes observed in many of the rare earths can be traced to the intricate form of the generalized susceptibility function. Assuming free electron bands in Eq. 19 yields the result

$$J_{ij} = \frac{8mI^2 |U^4(R_i)| k_f^4}{(2\pi)^3 \hbar^2} \frac{x \cos x - \sin x}{x^4} \qquad (21)$$

$$x = 2k_f R_{ij}$$

where k_f is the magnitude of the Fermi wavevector. This relation allows for various interaction strengths, both in magnitude and sign, depending

on the inter-atomic separation R_{ij}. Unfortunately, free electron bands are a very poor approximation to rare earth bands, and this relation is not particularly valid. This example does serve to illustrate one of the complex oscillatory forms which the generalized susceptibility can take. A more realistic approximation to the rare earth Fermi surfaces, crudely represented by a cylinder with flat ends separated by k_a, along with parabolic electron bands, gives the result

$$\chi(q) = \chi(0)1/t[\ln(1 + t/1 - t)]$$
$$t = q/k_a \tag{22}$$

for the generalized susceptibility.

The generalized susceptibility provides a description of the response of the conduction electrons to the internal field generated by the localized magnetic moments. One aspect of the indirect exchange interaction is that it leaves the conduction electrons polarized. This polarization of the conduction electrons will contribute to the net magnetization. This contribution to the net magnetization is given by Liu (13) as

$$M = -3N'J(\bar{Q})\mu_B\langle S\rangle/4E_f \tag{23}$$

where M is the magnetization, N' is the number of conduction electrons, $\langle S\rangle$ is the average ionic spin, and E_f is the Fermi energy. It is seen from this relation that the conduction electron contribution to the magnetization is proportional to the average ionic spin.

The generalized susceptibility also provides some basis for understanding the ordering temperatures observed in the rare earths. Magnetic

ordering will occur when the strength of the exchange interaction becomes comparable with thermal energies. A simple mean field theory gives the result

$$k_b T_0 = 2/3\ J(Q)S(S + 1) \tag{24}$$

where T_0 is the initial ordering temperature.

The indirect exchange coupling will also be reflected in the transport properties of the materials. Using a free electron model, Yosida (14) has shown that the change in electrical resistivity of a nonmagnetic host metal upon the addition of a small amount of solute with a localized moment is given approximately by

$$\Delta\rho = \frac{3}{2}\frac{\pi m}{\hbar E_f}\frac{N_i}{N^2 e^2}\left[A^2(0) + J^2(0)S(S + 1)\right] \tag{25}$$

where N_i is the number of solute atoms, N is the number of host atoms, and A(0) is a direct overlap integral, a term representing the usual impurity scattering due to changes in the electrostatic potential.

Thus, it has been seen that the indirect exchange interaction, mediated by the conduction electrons, gives rise to an interaction that may be viewed as an effective direct exchange interaction. This interaction, under certain simplifying assumptions, accounts for the intricate ordering schemes observed in the rare earths. It sheds some light of understanding on the resulting conduction electron polarization. It predicts the initial ordering temperatures. Finally, it provides the basic scattering interaction required for understanding the effects of magnetic solutes on the transport properties.

C. The de Gennes Hypothesis

In 1958, P. G. de Gennes (15) suggested that, due to the strong spin-orbit coupling observed in the rare earths, certain modifications should be made in the theory of the indirect exchange coupling mechanism. In the presence of strong spin orbit coupling, the L and S momentum vectors will precess together about the direction of the total momentum vector J. Because of this effect, de Gennes suggested that the spin vector S appearing in Eq. 12 should be replaced by its time averaged value. This time averaged value will simply be the projection of $\bar{S}$ and $\bar{J}$. That is, the term $\bar{\sigma}_i \cdot \bar{S}_j$ should be replaced by the expression

$$\bar{\sigma}_i \cdot \bar{J}_j \frac{\bar{S}_j \cdot \bar{J}_j}{J(J+1)} .$$

The term $\bar{S}_j \cdot \bar{J}_j$ can be easily calculated using the expression

$$\bar{S} \cdot \bar{J} = \frac{1}{2} (J^2 + S^2 - L^2).$$

The result of this calculation is that the term $\bar{\sigma}_i \cdot \bar{S}_j$ is replaced by the expression $(g - 1)\bar{\sigma}_i \cdot \bar{J}_j$, where g is the Lande g factor previously mentioned. The results of this modification appear in all of the results of the theory previously discussed. Equation 19 becomes

$$H_{int} = -\sum_{i,j} J_{ij}(g_i - 1)(g_j - 1)\bar{J}_i \cdot \bar{J}_j , \qquad (26)$$

Equation 24 becomes

$$k_b T_0 = \frac{2}{3} J(\bar{Q})(g - 1)^2 J(J + 1) , \qquad (27)$$

and Eq. 25 becomes (16)

$$\Delta\rho = \frac{3}{2}\frac{m}{hE_f}\frac{N_i}{N^2e^2}\left[A^2(0) + J^2(0)(g-1)^2J(J+1)\right] . \qquad (28)$$

It is inherent in de Gennes' argument that the strength of the spin-orbit interaction is much stronger than the strength of the exchange interaction. The Hamiltonian of the spin-orbit interaction is given by the expression

$$H_{s-o} = \sum_i \xi(r_i)\bar{l}_i \cdot \bar{s}_i \qquad (29)$$

$$\xi(r_i) = \frac{\hbar^2}{2m^2c^2}\frac{1}{r_i}\frac{dV}{dr_i}$$

where i runs over the various electrons. In the presence of forces which are central or spin-spin, all states with the same L and S are degenerate regardless of the value of J. This degeneracy in the various J states is removed by the noncentral spin-orbit interaction. Thus, the spin-orbit interaction splits the various J multiplets. The energy separation to the next excited multiplet can be calculated by treating the spin-orbit term as a perturbation. To first order, this separation is given by Elliott (17) for the rare earths as

$$\Delta = \langle\xi\rangle(J+1)/2\ S \qquad \text{shell less than half full}$$
$$\Delta = \langle\xi\rangle J/2\ S \qquad \text{shell more than half full} \qquad (30)$$

where $\langle\xi\rangle$ is the average of the single electron spin-orbit coupling over the 4f wavefunctions. If the value of $\langle\xi\rangle$, which is a measure of the strength of the spin-orbit interaction, is much larger than the value

of the exchange constant, it is appropriate to first deal with the spin-orbit interaction as a perturbation. In this case the $\overline{J} \cdot \overline{J}$ form of the exchange interaction results. If, however, the exchange constant is found to be much larger than the value of $\langle\xi\rangle$, the exchange interaction would dominate. Under these circumstances the $\overline{S} \cdot \overline{S}$ form of the exchange interaction would be indicated. The value of the separation of the multiplets has been measured spectroscopically (18). For Nd, which has a typical separation of 1900 cm^{-1}, the value of $\langle\xi\rangle$ found from Eq. 30 is of the order of 0.13 eV. Estimates of the value of the exchange constant have been calculated by Liu (13) based upon Curie temperature measurements in alloys. This estimate indicates that the value of the exchange constant is of the order of 0.2 eV. Thus, it is seen that the strengths of the two interactions are comparable, and the validity of the de Gennes hypothesis is not at all obvious. Consequently, it is left to further experimentation to determine the appropriate form of the exchange interaction.

III. EXPERIMENTAL PROCEDURE

A. Design of Magnetometer

In order to perform measurements of the saturation magnetizations of light rare earth-gadolinium single crystal alloys, a vibrating sample magnetometer was designed and built. The magnetometer was of the Foner type (19), with the general design features shown in Figure 1.

The general principles of operation are as follows. The sample under measurement is oscillated by driving the quartz sample rod at audio frequencies via an electromechanical transducer. The subsequent motion of the sample generates an alternating voltage in the pickup coils which is ideally proportional to the magnetization of the sample, the frequency of the motion, and the amplitude of the motion. In order to eliminate the frequency and amplitude dependence of the signal, a reference generator driven by the transducer is introduced. The voltage from the reference generator will have the same amplitude and frequency dependence as the voltage due to the sample. The reference voltage is then phase shifted by 180° and a fraction added to the sample voltage. The fraction of reference voltage required to achieve a null will then be proportional to the magnetization of the sample under measurement. This design tends to eliminate the effects of instabilities in the amplitude and frequency of the motion.

The details of the sample rod and sample holder are shown in Figure 2. The sample rod was constructed of two pieces of quartz cemented together with stycast. Quartz was chosen due to its low thermal

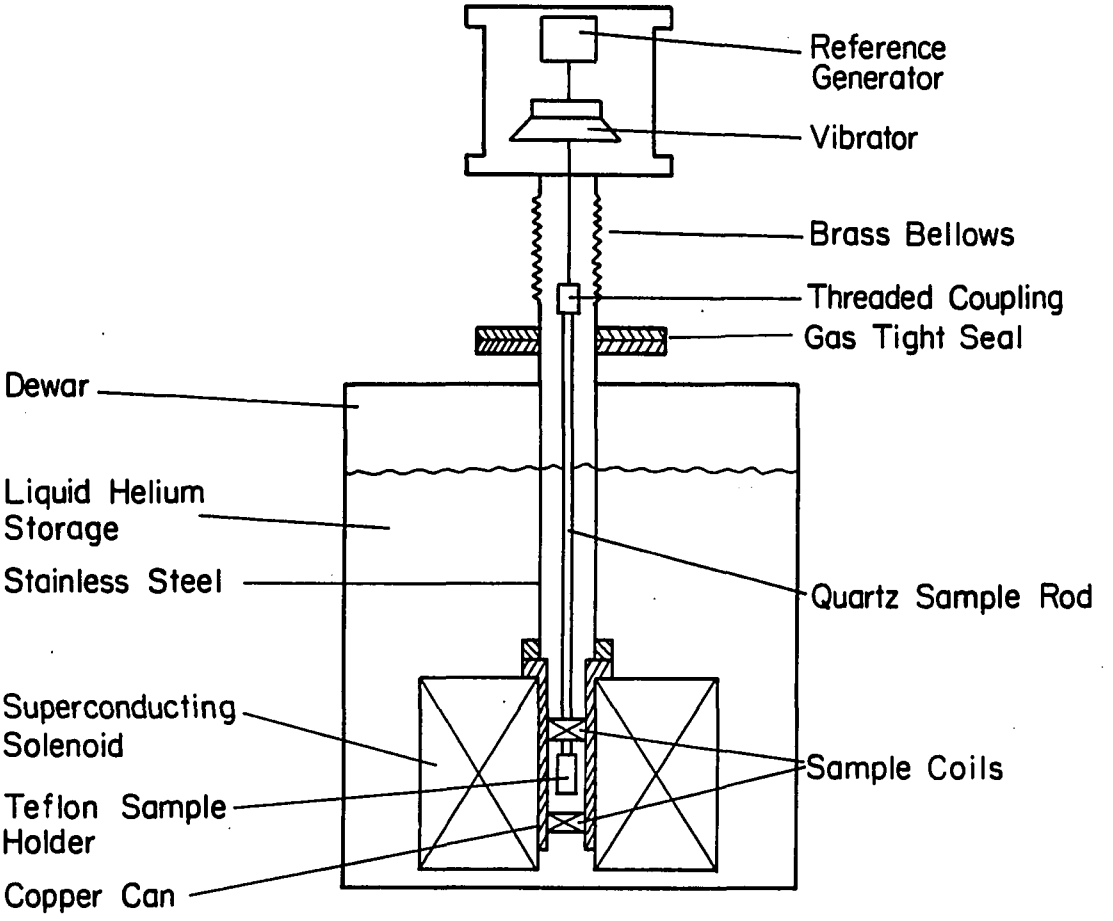

Figure 1. The general features of the vibrating sample magnetometer

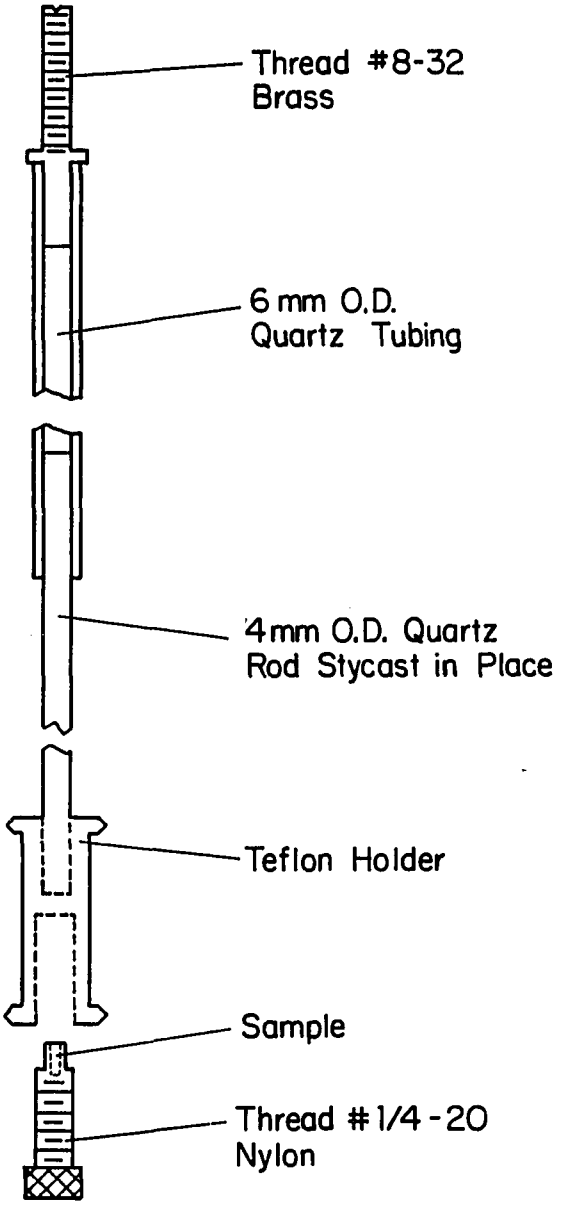

Figure 2. Details of the sample rod and sample holder

expansion and rigidity. The upper piece was a hollow tube, while the lower piece was a solid rod which telescoped into the upper piece. The telescoping design is advantageous due to the fact that it tends to eliminate transverse modes of oscillation along the rod. The sample holder was machined out of Teflon and cemented to the sample rod with stycast. Teflon was chosen due to its nearly negligible magnetic properties.

The electromechanical transducer was made up of the magnet and voice coil of a Radio Shack 100 watt loudspeaker. The entire drive mechanism and reference generator assembly was mounted in a can. The can was in turn mounted on a rack allowing for vertical positioning via a remotely controlled low speed motor-reduction gear assembly. The sample could thus be centered between the pickup coils by moving the can up or down until a maximum was obtained in the signal voltage.

The pickup coils were made up of two astatically wound coils of axial symmetry. Details are given in Figure 3. The coils were made up of approximately 10,000 turns each of #46 copper wire. The coils were balanced to minimize the effects of fluctuations in the external magnetic field. The coil geometry was chosen to give the maximum sensitivity while at the same time giving the minimum sensitivity to errors in sample positioning. In an attempt to minimize the effects of image poles (to be discussed later), the entire coil package was mounted inside a copper can. In order to insure that there was no relative motion between the coil package and the solenoid, the coil package was glued to the solenoid

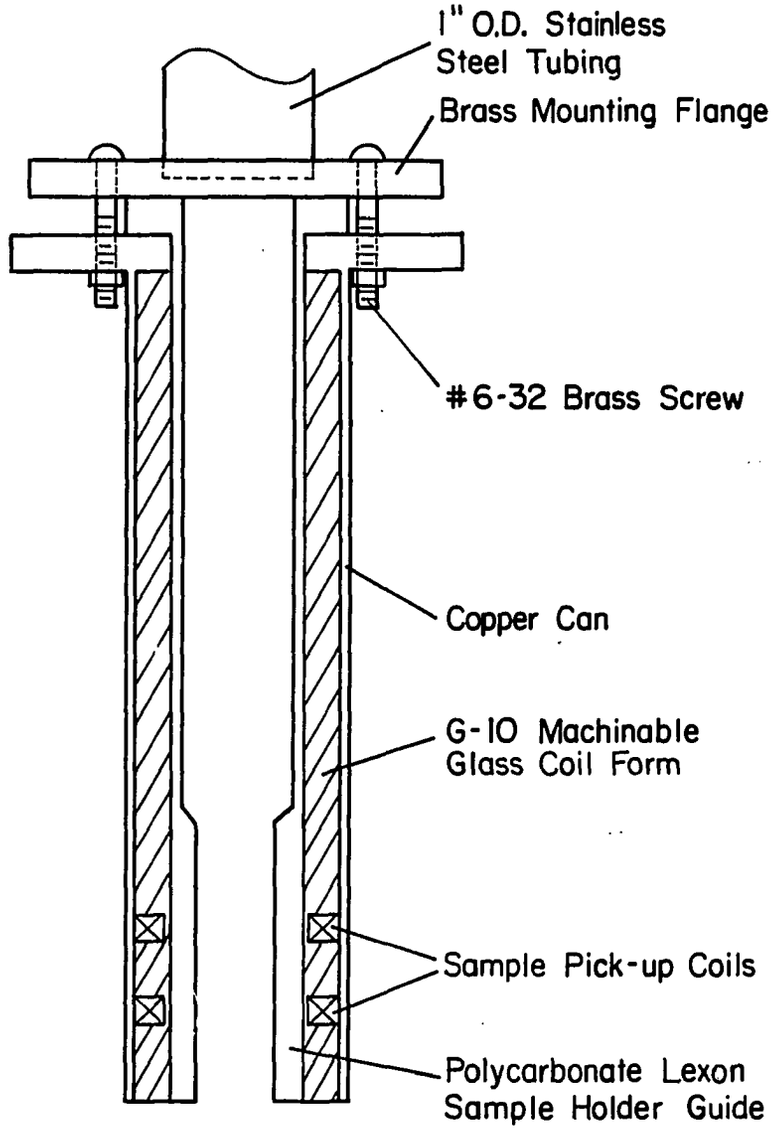

Figure 3. Details of the sample pickup coil package

by coating it with vacuum grease before fitting it in place. When the apparatus was cooled to liquid helium temperatures, the grease froze, solidly anchoring the coils to the solenoid.

Details of the reference generator are given in Figure 4. The standard sample was made up of a piece of Alnico permanent magnet with approximately the same geometry as the samples to be measured. The two reference coils were wound with a geometry nearly identical to the pickup coils. The standard sample was centered between the reference coils by moving it up or down via a threaded coupling to the drive rod and looking for a maximum in the reference voltage. The entire assembly was mounted in the housing of a Ling Electronics model V47/3 vibration generator. This housing was chosen due to the fact that it was fabricated from metal which was magnetically very soft, and thus shielded the reference mechanism from the effects of stray magnetic fields.

High external magnetic fields were generated using an Intermagnetics General Corp. Model SO-9192B superconducting solenoid wound out of Nb_3Sn ribbon. The magnet was capable of producing fields in excess of 122 kOe in a bore of approximately 1.5 inches in diameter. The magnet was driven by an Intermagnetics General Corp. Model IGC-150MM power supply.

The magnitude of the applied magnetic field was determined by using a magnetoresistance probe installed in the midplane of the magnet and calibrated by the manufacturer. The stated reproducibility of the probe was 0.1%. Current was provided to the probe by a constant current supply. Voltage was measured by a Leeds and Northrup type K-3 potentiometer.

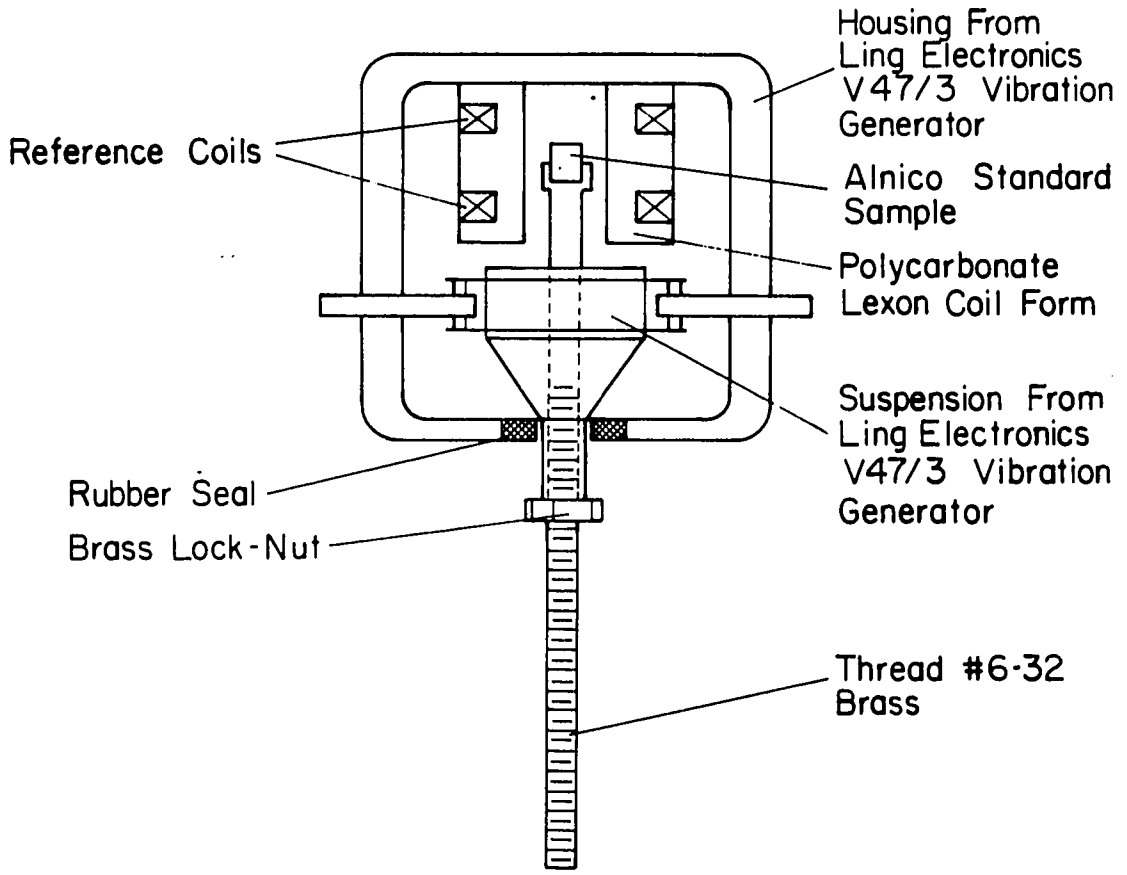

Figure 4. Details of the reference generator

Details of the electronic circuits are given in Figure 5. The motion of the smaple will produce an ac voltage in the pickup coils which is characterized by the same frequency as the driving voltage. Similarly, the motion of the standard sample will produce an ac voltage in the reference coils with an identical waveform as the signal voltage. Ideally, since the standard sample and the unknown sample are both rigidly fixed to the same rod, the reference voltage and sample voltage would have the same phase. In reality, loss mechanisms in the coils and nearby magnetic materials as well as phase shifts produced by interconnecting cables give rise to a phase difference between the reference and signal voltages which is not necessarily constant. For this reason, a device was required which would allow for the continuous shifting of the reference voltage phase, while at the same time leaving the amplitude unaltered.

Details of the phase shifting circuit are given in Figure 6. The design utilized an active phase shift using an RC circuit to produce a continuous phase shift in the reference voltage. In this case, the resistor was the variable element. The phase shift of an RC circuit will be amplitude constant only if the circuit is not under load. This situation was achieved by utilizing the ideal impedance characteristics of operational amplifiers. In order to obtain the desired sensitivity of the apparatus, a fixed gain amplifier was included after the phase shifting circuit. Tests of the phase shifting circuit indicated that the circuit would produce a phase shift of approximately 100°, with a variation in output amplitude of less than 0.1% over this range.

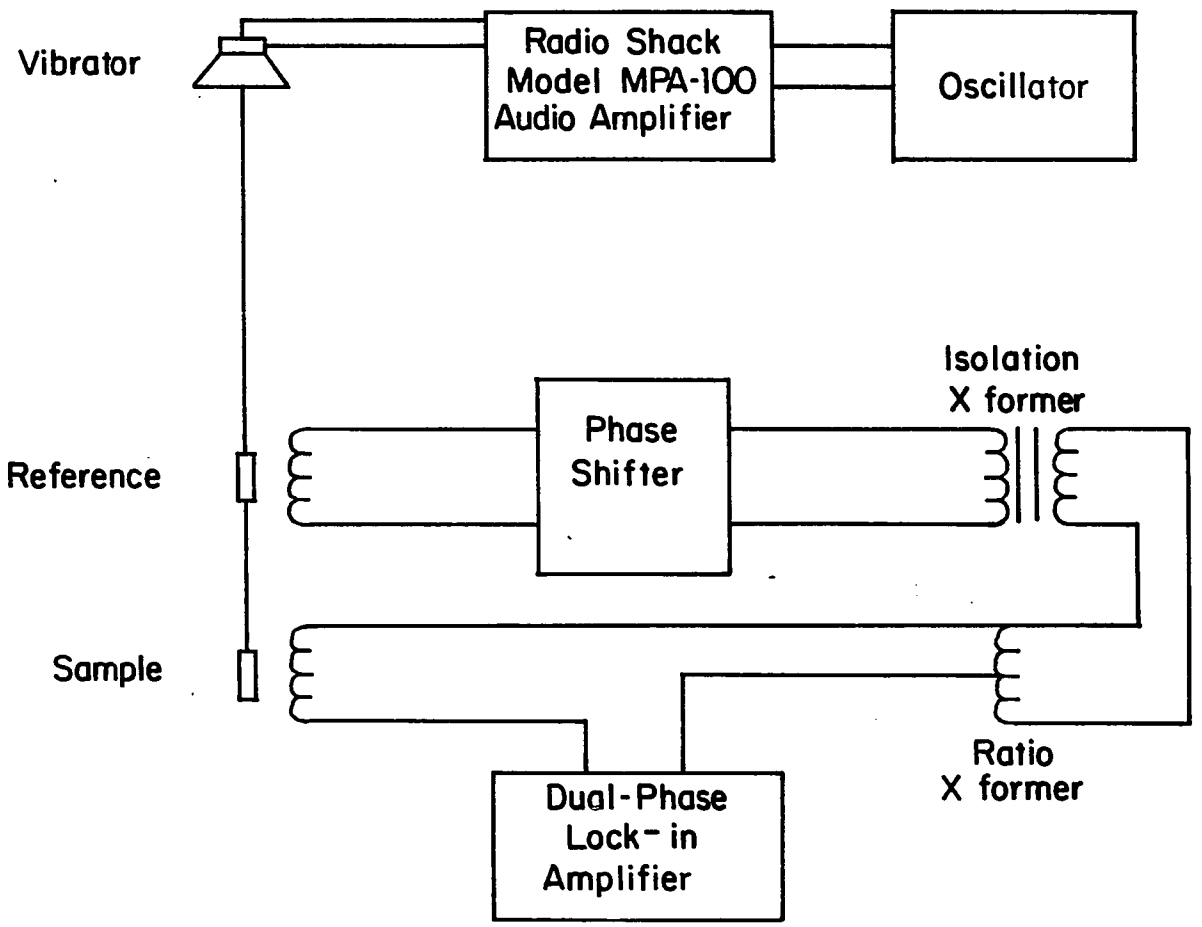

Figure 5. The complete circuit diagram for the vibrating sample magnetometer

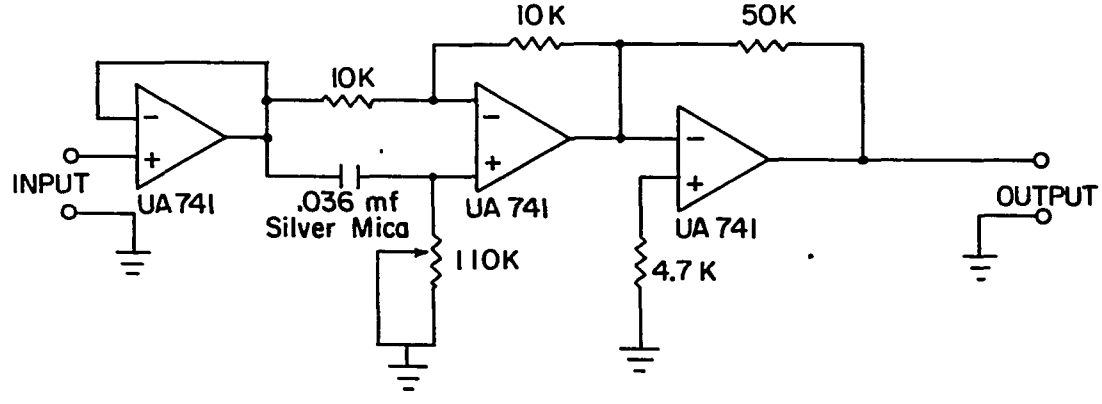

Figure 6. The circuit diagram of the phase shifter

The fraction of the reference voltage added to the sample voltage was selected by using a Gertsch Model 1011 ratio transformer. A ratio transformer was used because it provided a known fraction of reference voltage with no phase change.

Detection of the null condition was provided by a Princeton Applied Research Corp. Model 5204 dual phase lock-in amplifier. The lock-in amplifier is a device which is essentially a narrow band detector which detects a.c. voltages that are phase related to a reference voltage. The Model 5204 was ideally suited for this application for a number of reasons. First, the Model 5204 is provided with circuitry which allows for the detection of the component of the incoming signal which differs in phase from the reference voltage by a variable amount. This capability was extremely important in this measurement. The lock-in was referenced by the same voltage that drove the loudspeaker. However, due to phase changes resulting from previously mentioned processes, the voltage from the pickup coils was shifted by approximately 43° from the lock-in reference voltage. This phase shift could thus be compensated for by observing the component of the incoming voltage which was phase shifted by 43° from the lock-in reference voltage. This component of the incoming voltage is known as the in-phase component. The second necessary characteristic of the Model 5204 was its dual phase capability. Circuitry was provided which enabled the lock-in to simultaneously display the in-phase component as well as the 90° out-of-phase component of the incoming voltage. Obtaining a simultaneous null in both the in-phase and the 90°

out-of-phase components of the incoming voltage insured that the reference coil voltage was exactly 180° out of phase with the pickup coil voltage. This situation could only be achieved by adjusting both the fraction and phase of the reference coil voltage. The third desirable feature of the Model 5204 was its frequency tracking capabilities. This feature enabled the lock-in to function optimally, even in the presence of frequency drifts of the reference voltage. Finally, the detection sensitivity of the Model 5204 was very good (approximately 10 nV full scale). Thus, the Model 5204 dual phase lock-in amplifier provided an ideal null detector for this measurement.

The driving voltage to the loudspeaker was provided by a Hewlett Packard Model 200 JR audio oscillator driving a Radio Shack Model MPA-100 100 watt audio amplifier. The driving frequency was set at approximately 110 Hz with a power output of approximately 90 W. This particular frequency was chosen because there are no ordinary harmonics from local power sources at this frequency, and in addition, it was adequately removed from mechanical resonance frequencies of the drive speaker-sample rod system. A power output of 90 W was required in order to drive the sample rod at sufficiently high amplitudes (approximately 0.5 mm).

Temperature control of samples under measurement was provided by immersing the sample directly in the liquid helium bath. Thus, all measurements were performed at a temperature of 4.2 K.

B. Calibration

The instrument heretofore described measured the magnetization of an unknown sample relative to the output of a reference generator.

Therefore, the measurements were relative measurements. In order for these relative values to be converted to absolute values, the magnetometer must be calibrated relative to some known material.

The quantity actually measured with this instrument is the fraction of reference voltage fed back by the ratio transformer. This quantity, the dial reading of the ratio transformer DR, is ideally proportional to the magnetization. Thus, if a sample with a known magnetization gives a specific reading DR_c (the calibration dial reading), the calibration constant K can be determined from the following relation:

$$K = \frac{\sigma m}{DR_c} \tag{31}$$

where σ is the known magnetization of the calibration standard in emu/gm, m is the mass in grams, and DR_c is the calibration dial reading at the field and temperature corresponding to σ. Thus, the value of the magnetization of an unknown sample, σ', is given in absolute units by the expression:

$$\sigma' = \frac{DR'K}{m'} \tag{32}$$

where DR' is the ratio transformer dial reading of the unknown sample, m' is its mass in grams, and K is the calibration constant given by Eq. 31.

In reality, a major difficulty is encountered in this calibration scheme. In addition to the considerations discussed above, one must also take into account an effect known as the "image pole" effect (20). This effect has its origin in "image poles" similar to those encountered

in electrostatics. The sample under measurement is in the vicinity of the diamagnetic windings of the superconduction solenoid, giving rise to a magnetic boundary value problem. The solution of this boundary value problem can be obtained by the introduction of magnetic image poles, in a manner almost identical with the well-known electrostatics problem. Since the image poles oscillate along with the sample, with a possible phase factor, the signal generated in the pickup coils will be considerably enhanced. In order to alleviate the effect of the image poles, the pickup coils were enclosed in a copper can machined out of high purity oxygen free copper. The image poles are actually a result of the penetration of the dipole field of the sample (which is oscillating at audio frequencies) into the magnet, where it is "reflected" back into the pickup coils. The copper can effectively screen out this field. The penetration depth of 100 Hz electromagnetic radiation in high purity copper at 4.2 K was estimated to be approximately 2 mm. For complete shielding, one would ideally use a copper can of several penetration depths of thickness. Unfortunately, due to space limitations of the magnet bore, the copper can of this particular instrument was only approximately 1.5 mm thick, and some signal enhancement was observed.

In general, the contribution due to the image poles is proportional to the sample magnetization and the contribution due to the image poles is given by

$$M_{image} = M_{sample}\, I(\mu) \tag{33}$$

where M_{image} is the strength of the image pole contribution, M_{sample} is the magnetization of the sample, and $I(\mu)$ is the coupling constant, which in general is a function of solenoid geometry and the permeability of the superconducting ribbon μ. The observed signal is then given by

$$DR_{obs} = \frac{M_{sample} m_{sample}}{K} [1 - I(\mu)] \tag{34}$$

where K is given by Eq. 32, and m_{sample} is the mass of the sample.

In general, the permeability of a type II superconductor such as Nb_3Sn is a complex function of the field H. Thus, $I(\mu) \rightarrow I'(H)$ in Eq. 34 to yield

$$DR_{obs} = \frac{M_{sample} m_{sample}}{K} [1 - I'(H)] \tag{35}$$

or alternatively

$$DR_{obs} = \frac{M_{sample} m_{sample}}{(K'(H)} \tag{36}$$

where

$$K'(H) = \frac{K}{1 - I'(H)} . \tag{37}$$

Thus,

$$M_{sample} = DR_{obs} \frac{K'(H)}{m_{sample}} . \tag{38}$$

It can be seen by comparing Eq. 38 with Eq. 32 that the net effect of the image poles is to give a field dependence to the calibration constant K.

From the preceding discussion, it becomes apparent that the calibration function K'(H) can be determined by performing measurements on a

calibration standard which has a known magnetization at all fields. K'(H) is then given by

$$K'(H) = \frac{DR_c(H)}{M_c(H)} m_c \qquad (39)$$

where $DR_c(H)$ is the ratio transformer dial reading of the calibration standard at the field H, m_c is the mass of the calibration standard, and $M_c(H)$ is the known magnetization of the calibration standard at the same field H.

The calibration standard selected for this particular experiment was a piece of high purity iron produced by the U.S. Steel Corp. Iron was selected primarily for two reasons. First, the magnetic moment of iron is comparable to that of the samples measured (approximately 221 emu/gm). Secondly, the magnetization of iron has been measured out to high fields (21,22), and thus was known for all fields under measurement.

The calibration function K'(H) was determined in accordance with the procedures described above out to fields of approximately 123 kOe. Values of the calibration function were found to reproduce to within 0.2% from run to run. In order to check the reliability of the calibration procedure previously described, the magnetization of a high purity nickel sample was measured out to applied fields of approximately 123 kOe. The value of the saturation magnetization obtained through these measurements agreed to within 0.2% of the accepted value determined by Danan et al. (22). In addition, the calibration function was determined using

a high purity iron standard obtained from the National Bureau of Standards which had a slightly larger sample geometry than the U.S. Steel iron standard. The calibration functions obtained using these two separate standards agreed to better than 0.2% over the entire range of applied fields. The calibration function was found to vary from approximately 150 emu at low fields to approximately 140 emu at high fields, and is shown in Figure 7.

C. Magnetization Measurements

In this study, the magnetizations of various single crystal alloys of light rare earths with gadolinium were measured at a temperature of 4.2 K in applied fields from 0 to 123 kOe in order to extract the saturation magnetizations. It has been common practice to expand the magnetization of ferromagnetic materials as a series containing various powers of the internal field. Thus, the magnetization of a ferromagnetic material is given approximately by the expression

$$\sigma = \sigma_0 + \chi H_{int} + \alpha H_{int}^{-1} \tag{40}$$

where σ is the magnetization per gram, H_{int} is the internal field, and σ_0 is the saturation magnetization per gram. Inclusion of the term αH_{int}^{-1} was originally suggested by Weiss (23), and is related to domain wall movement. χ, the susceptibility term, arises from the Pauli susceptibility as well as from a crystal defect contribution (21), and can be quite a significant contribution to the magnetization at fields in excess of 30 kOe.

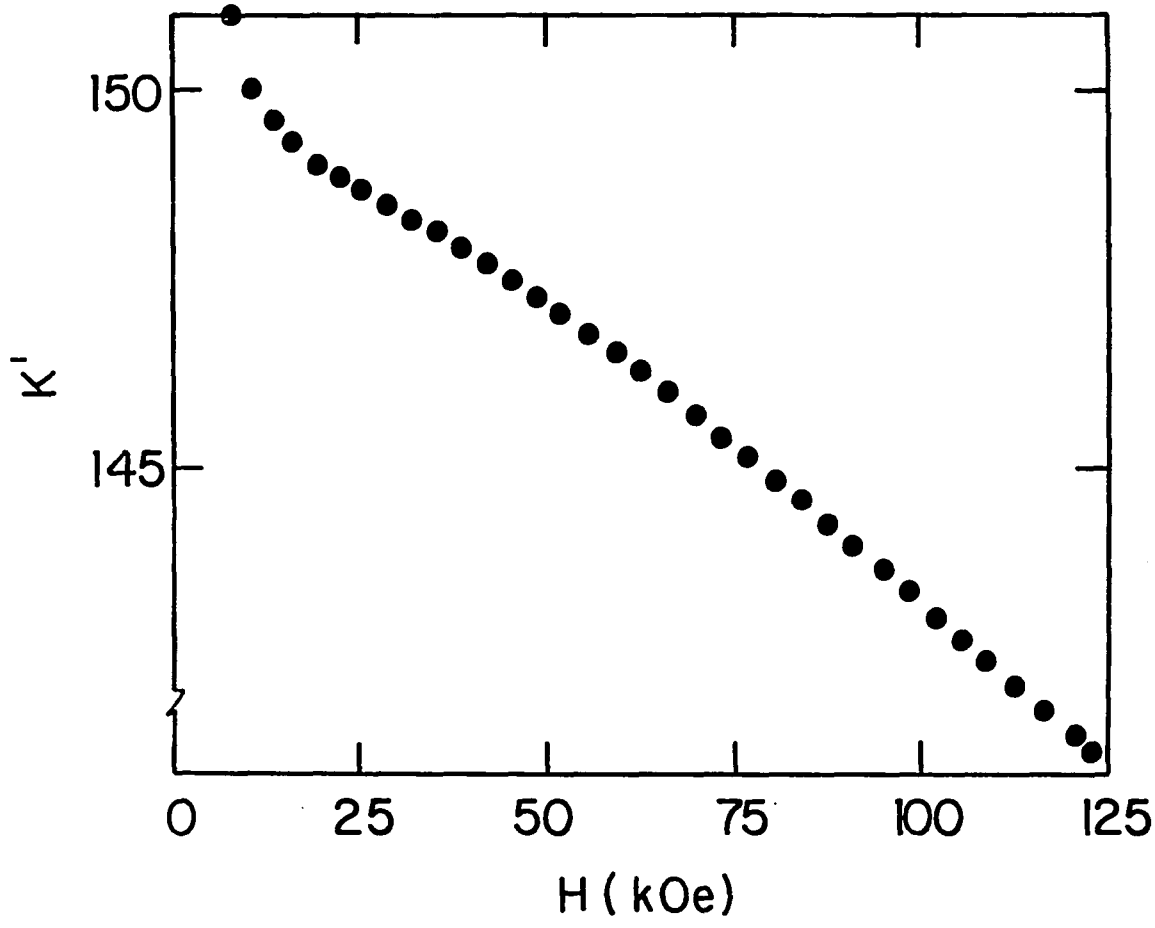

Figure 7. The calibration function as a function of field

Demagnetization effects give rise to a magnetic field within the sample which is slightly less than the applied field. The internal field of a ferromagnetic sample is given by

$$H_{int} = B = H - N\,I \tag{41}$$

where H_{int} is the internal field, H is the applied field, I is the intensity of the magnetization, and N is a geometric factor known as the demagnetization factor. The magnetization per gram is given by

$$\sigma = I/d \tag{42}$$

where d is the density. Thus,

$$H_{int} = H - Nd\sigma. \tag{43}$$

Various demagnetization factors as a function of sample geometry have been calculated and are given by Bozorth (24).

After the magnetization data were corrected to internal fields, the data were fit to Eq. 40 using a curve fitting routine given by Bevington (25). The value of σ_0 returned by this fitting process was taken to be the value of the saturation magnetization.

All measurements were performed at a temperature of 4.2 K. The value of the saturation magnetization at 4.2 K was taken to be the same as the value at 0 K. The temperature dependence of the saturation magnetization has been theoretically predicted by several workers (10,26, 27), the most notable result being the Bloch $T^{3/2}$ law predicted by spin wave theory. The result may be stated in the form (24)

$$\frac{\sigma(T)}{\sigma(0)} = 1 - a\left(\frac{T}{T_c}\right)^{3/2} \tag{44}$$

where $\sigma(T)$ is the saturation moment per gram at temperature T, $\sigma(0)$ is the saturation moment per gram at 0 K, T_c is the Curie temperature, and a is a constant which is experimentally found to be of the order of 0.11. The Curie temperatures of the samples examined in this study are all estimated to be of the order of 250-260 K. Using Eq. 44, the difference between the saturation moment at 4.2 K and 0 K is expected to be of the order of 0.04%, well below the accuracy of the measurements. Thus, the assumption that the saturation moment as measured at 4.2 K is identical to the saturation moment at 0 K is justified.

D. Sample Preparation

The ideal sample composition to be used in this investigation would be a fifty-fifty mixing of light rare earth with gadolinium. Unfortunately, only relatively small percentages of light rare earth may be alloyed with gadolinium before mixed phases occur. Accordingly, the compositions of the alloys used in these measurements were those consisting of the highest percentage of light rare earth possible while still maintaining the pure hcp phase.

The alloys used in this work were prepared by B. J. Beaudry of the Materials Science and Engineering section of the Ames Laboratory USDOE. In all cases, initial preparation consisted of arc melting together the carefully weighed constituents over a copper hearth.

Two separate batches of gadolinium were used in making up the samples. The neodymium samples were made up using Gd I. Mass spectrometric and vacuum fusion analysis of Gd I indicated the presence of approximately

51 ppm Fe, 6 ppm Cl, 22 ppm Ni, 0.6 ppm Na, 0.5 ppm Ca, 3.7 ppm Cu, 3 ppm Ta, and 3 ppm P. All rare earth impurities were less than 10 ppm, with the exception of 140 ppm Tb. In addition, 933 ppm O, 314 ppm N, 622 ppm H, and 301 ppm C were detected. No other impurities were detected. All concentrations are given in atomic ppm. Similar analysis of the starting Nd gave comparable impurity levels with the exception of only 20 ppm Tb and 405 ppm O. Single crystals were obtained in the arc melted button by first peening the button and then annealing it for 24 hours in the strong temperature gradient region of an electric furnace at a mean temperature of 1100 C. The crystals were then aligned by the Laue technique, and cut to dimensions of approximately 2 x 2 x 5 mm with a spark cutter and diamond saw. The crystals were then electropolished. X-ray analysis indicated the pure hcp structure.

The praseodymium samples were prepared with Gd II. Mass spectrometric and vacuum fusion analysis of Gd II indicated the presence of 41 ppm Fe, 2 ppm Cl, 5 ppm Ni, 6 ppm Cu, and 2 ppm Al. Rare earth impurities were all less than 3 ppm. Additional impurities of 344 ppm O, 45 ppm N, 622 ppm H, and 131 ppm C were detected. No other impurities were detected. Similar analysis of the starting Pr gave comparable results. The preparation of the first praseodymium samples, known as alloy I, was somewhat irregular, and in light of the fact that these samples gave anomalous results, a second set of samples, known as alloy II were prepared. The alloy I samples were prepared by first peening the arc melted button and then annealing it for two days in the strong

temperature gradient region of an electric furnace at a mean temperature of 1150 C. This process gave very small grains. The ingot was then re-peened and annealed at an average temperature of 1080 C. This produced large grains. The crystals were then aligned by the Laue technique and cut to dimensions of approximately 2 x 2 x 5 mm with a spark cutter and diamond saw. The crystals were then electropolished. X-ray analysis indicated the pure hcp structure. Subsequent metallographic analysis indicated that the samples were indeed single phase single crystal. The alloy II samples were prepared by first peening the arc melted button and then annealing it for seven days at a mean temperature of 1080 C in a temperature gradient. This produced large grains. The crystals were then aligned, cut to dimensions of approximately 2 x 2 x 5 mm, and then electropolished. X-ray analysis indicated the pure hcp structure.

The cerium samples were prepared with Gd II. Analysis indicated the presence of impurities comparable to those found in Gd II. The arc melted button was peened and then annealed for three days at an average temperature of 1140 C in a temperature gradient. The button was then cooled to 1110 C and held there for one day. This produced large grains. The crystals were then aligned, cut to dimensions of approximately 2 x 2 x 5 mm, and then electropolished. X-ray analysis indicated the pure hcp structure.

IV. RESULTS

A. Pure Gadolinium

As has been previously discussed, the object of this investigation has been to determine the validity or invalidity of the de Gennes hypothesis through measurements of the saturation magnetizations of alloys of light rare earths with gadolinium. In order to separate the conduction electron contribution from the ionic contribution to the saturation magnetization, the conduction electron contribution in the pure host gadolinium must be measured.

Gadolinium is the only rare earth which is a simple ferromagnet. The Curie temperature is 293.4 K and the direction of easy magnetization just below the Curie point is along the c-axis. The temperature dependence of the magnetic moment of single crystals has been measured at several internal fields by Nigh et al. (28). Their results indicate that the easy direction moves away from the c-axis to the basal plane at lower temperatures. These results have been confirmed by neutron diffraction observations made by Will et al. (29) and by Cable and Wollan (30). Saturation magnetization measurements were performed by Nigh et al. (28). They obtained a value of 0.55 μ_B/atom for the surplus moment, which is attributed to the conduction electron polarization. More recent measurements on electrotransported single crystals with very low oxygen content by Roeland et al. (21) and by White et al. (31) give a surplus moment of 0.63 μ_B/atom. This difference between the two values of the surplus mement is attributed to impurity effects, primarily oxygen.

The value of the surplus moment is critical in understanding the saturation magnetizations of the gadolinium alloys. The neodymium alloy was made up with a different batch of gadolinium than the praseodymium and cerium alloys. The gadolinium used to make up the neodymium alloy is known as Gd I and the gadolinium used to make up the praseodymium and cerium alloys is known as Gd II. Mass spectrometric and vacuum fusion analysis of Gd I indicate the presence of approximately 140 ppm (atomic) terbium, as well as 933 ppm (atomic) oxygen. Similar analysis of Gd II found no indications of terbium impurities. The oxygen impurity content was found to be 344 ppm (atomic).

In order to obtain the appropriate value of the surplus moment to be used with each of the alloys, saturation magnetization measurements were performed on a- and b-axis samples of Gd I and on a b-axis sample of Gd II. Results of these magnetization measurements, performed at 4.2 K, are given in Figure 8. As can be seen from the figure, no anisotropy was observed between the a- and b-axis samples. The solid curves are fits of the data to Eq. 40. The results of the latter are:

for Gd I a-axis

$$\sigma_0 = 272.7 \pm 0.8 \text{ emu gm}^{-1}$$

$$\chi = (7.4 \pm 5.6) \times 10^{-3} \text{ emu gm}^{-1} \text{ kOe}^{-1}$$

$$\alpha = -18.2 \pm 20 \text{ emu gm}^{-1} \text{ kOe}$$

for Gd I b-axis

$$\sigma_0 = 272.7 \pm 0.8 \text{ emu gm}^{-1}$$

$$\chi = (7.2 \pm 5.3) \times 10^{-3} \text{ emu gm}^{-1} \text{ kOe}^{-1}$$

$$\alpha = -24 \pm 8 \text{ emu gm}^{-1} \text{ kOe}$$

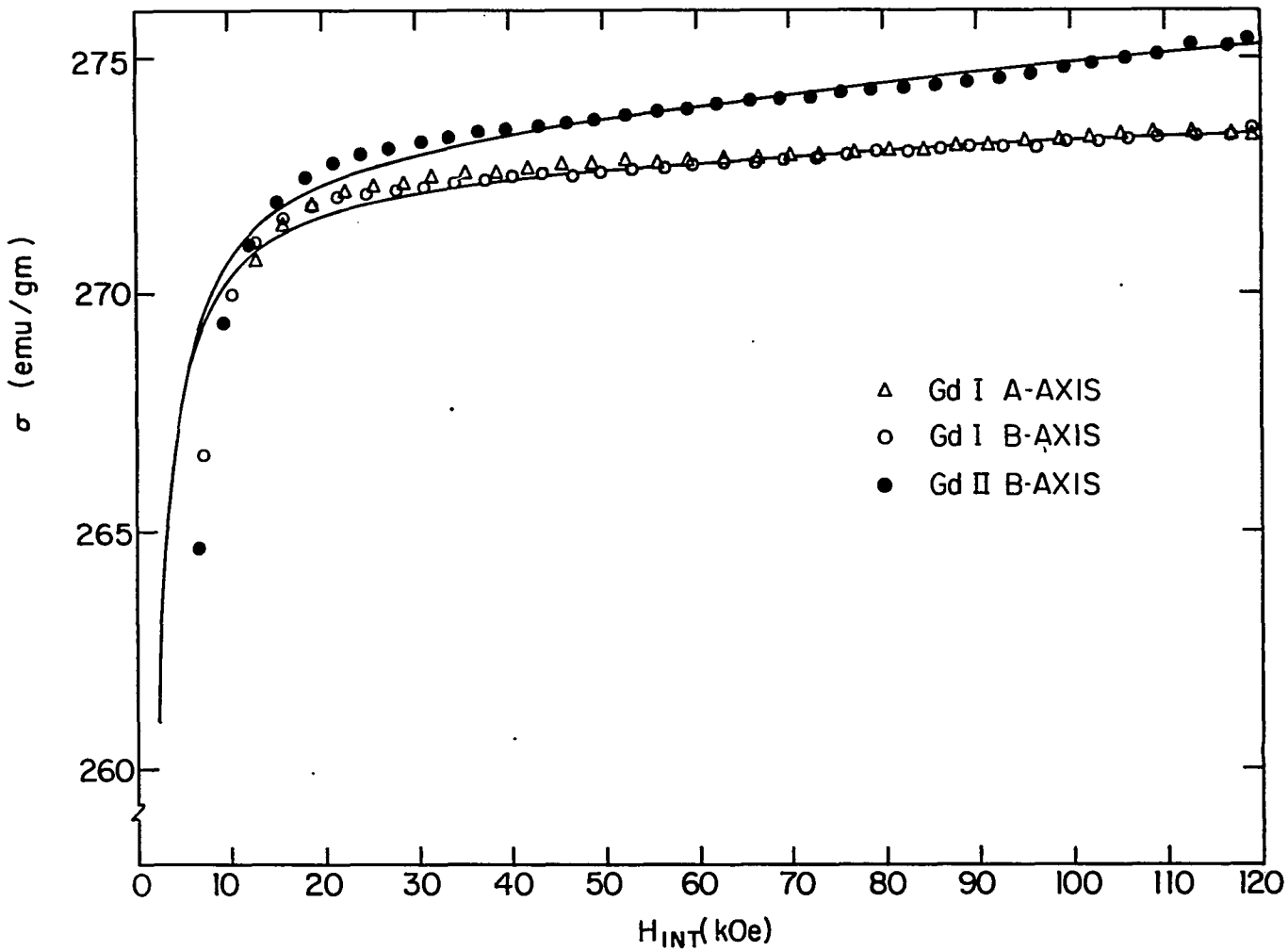

Figure 8. Isothermal magnetization of Gd I and Gd II as a function of internal field. The solid curves represent a fit of the data to Eq. 40

for Gd II b-axis

$\sigma_0 = 273.3 \pm 1.1$ emu gm^{-1}

$\chi = (1.9 \pm 1.4) \times 10^{-2}$ emu gm^{-1} kOe^{-1}

$\alpha = -27 \pm 11$ emu gm^{-1} kOe.

These values of the saturation magnetization correspond to values of 0.68 ± 0.03 μ_B/atom for Gd I and 0.70 ± 0.04 μ_B/atom for Gd II for the surplus moment. These values are significantly higher than the previously reported values. The reason for this difference is not well understood, but is believed to be related to impurities. Roeland et al. (21) obtained the values $\chi = (1.1 \pm 2.1) \times 10^{-3}$ emu gm^{-1} kOe^{-1} and $\alpha = -3.2 \pm 3.6$ emu gm^{-1} kOe for electrotransported samples, and $\chi = (20 \pm 1.4) \times 10^{-3}$ emu gm^{-1} kOe^{-1} and $\alpha = -8.9 \pm 1.1$ emu gm^{-1} kOe for nonelectrotransported samples. Thus, it is seen that the values of χ obtained in this measurement lie between the previously reported values while the value of α is somewhat higher. Again, this discrepancy may be related to impurities. Comparison of the values of the saturation moments of Gd I and Gd II indicate that the presence of high moment heavy rare earth impurities may be an important factor in the surplus moment. Roeland et al. (21) estimated the oxygen content of their electrotransported samples to be approximately 100 ppm (atomic), which is comparable to the oxygen content of the Gd II sample. They gave no indication of the rare earth impurity content in their samples. Rare earth impurities are relatively unaffected by the electrotransport process. Unfortunately, this must remain as idle speculation due to the errors involved in the present measurements.

B. 14.5% Nd in Gd

Some of the magnetic properties of Gd-Nd polycrystalline alloys have been reported by Fujimori et al. (32). The results of their saturation magnetization measurements indicated that the neodymium ions align with their moments antiparallel to the gadolinium moments, and carry a moment of $3.3 \pm 0.1\ \mu_B$/atom. This value is consistent with the value predicted by Eq. 3 of $3.27\ \mu_B$/atom.

Measurements of the isothermal magnetization as a function of field were performed on both a- and b-axis single crystals of an alloy of 14.5 atomic percent neodymium in gadolinium at a temperature of 4.2 K. Results of these measurements are shown in Figure 9. The solid curves are fits of the data to Eq. 40. The results of these fits are:

for the a-axis sample

$$\sigma_0 = 218.2 \pm 0.7 \text{ emu gm}^{-1}$$
$$\chi = (6.4 \pm 4.7) \times 10^{-2} \text{ emu gm}^{-1} \text{ kOe}^{-1}$$
$$\alpha = (-2.5 \pm 0.4) \times 10^{2} \text{ emu gm}^{-1} \text{ kOe}$$

for the b-axis sample

$$\sigma_0 = 218.4 \pm 0.7 \text{ emu gm}^{-1}$$
$$\chi = (4.1 \pm 2.9) \times 10^{-2} \text{ emu gm}^{-1} \text{ kOe}^{-1}$$
$$\alpha = (-1.6 \pm 0.8) \times 10^{1} \text{ emu gm}^{-1} \text{ kOe.}$$

These values of the saturation magnetization correspond to values of $6.07 \pm 0.03\ \mu_B$/atom and $6.08 \pm 0.03\ \mu_B$/atom for the average moment per atom of the a- and b-axis samples, respectively. As the figure shows, there is some anisotropy between the two directions, with the b-axis

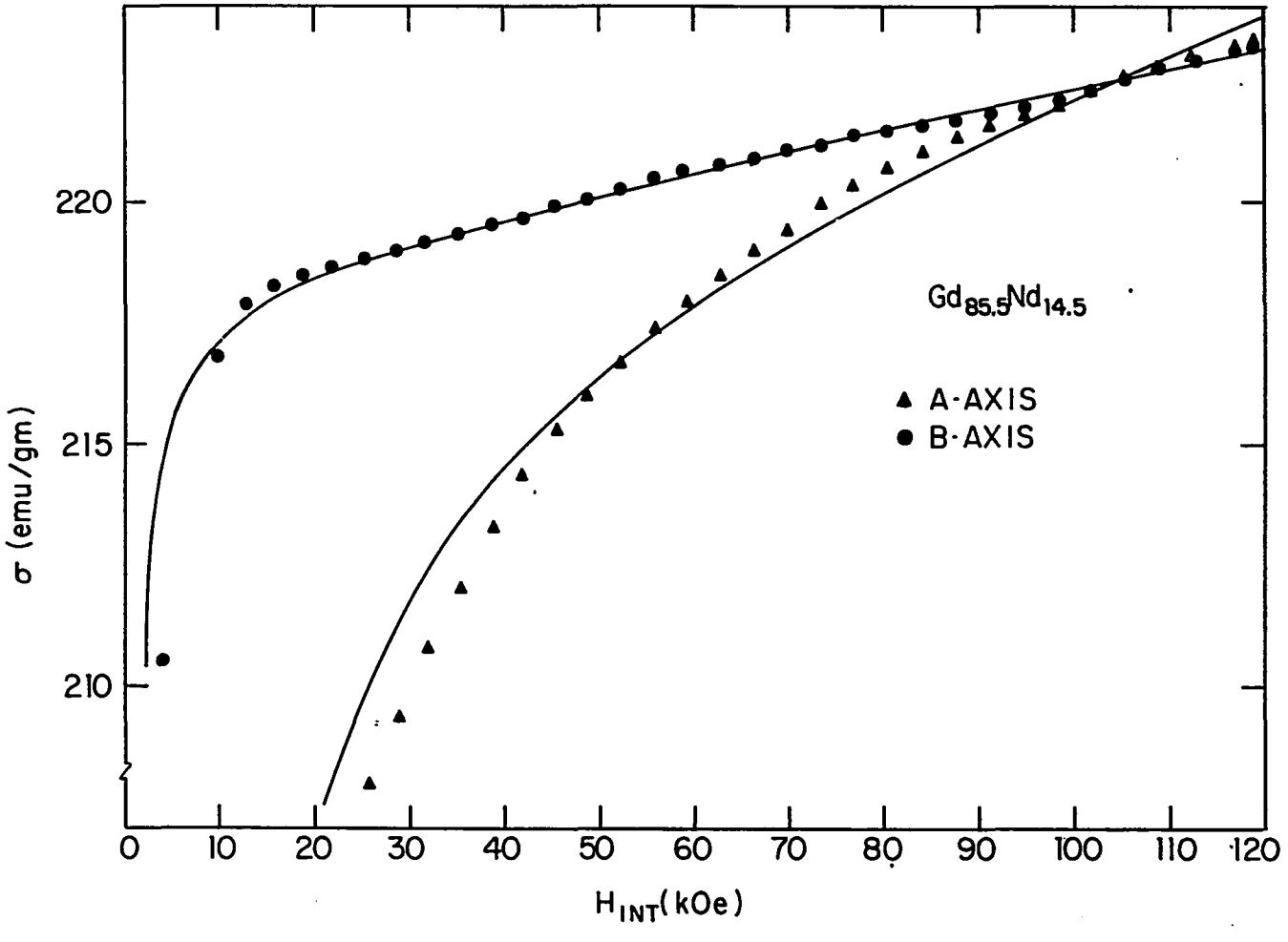

Figure 9. Isothermal magnetization of $Gd_{85.5}Nd_{14.5}$ as a function of internal field. The solid curves represent a fit of the data to Eq. 40

being the easier direction. Thus, the average saturation moment per atom for 14.5 atomic percent neodymium alloyed into gadolinium is taken to be $6.08 \pm 0.03\ \mu_B$/atom.

C. 11.0% Pr in Gd

Saturation magnetization measurements on a single crystal alloy of 9.0 atomic percent praseodymium in gadolinium have been reported by Legvold et al. (33). Their measurements indicated that the exchange field dominated the effects of the hexagonal crystalline electric fields. This was indicated by the result that the Pr ions carried the predicted moment of $3.20\ \mu_B$/atom aligned antiparallel to the Gd moments.

Isothermal measurements of the magnetization as a function of field were performed on both a- and b-axis single crystals of an alloy of 11.0 atomic percent praseodymium in gadolinium at a temperature of 4.2 K. Results of these measurements on the initial alloy, known as alloy I, are shown in Figure 10. As can be seen from the figure, the magnetization curves of these two samples are anomalous in that the magnetization of the b-axis sample is less than that of the a-axis sample out to internal fields of approximately 27 kOe. Beyond this point, the magnetization of the b-axis sample increases to a value approximately 0.8% higher than that of the a-axis sample at an internal field of 120 kOe. There is no known physical process which would account for this behavior in two samples of identical composition and structure, differing only in crystallographic orientation in the basal plane. The solid curves in Figure 10 represent fits of the data to Eq. 40. The results of these fits are:

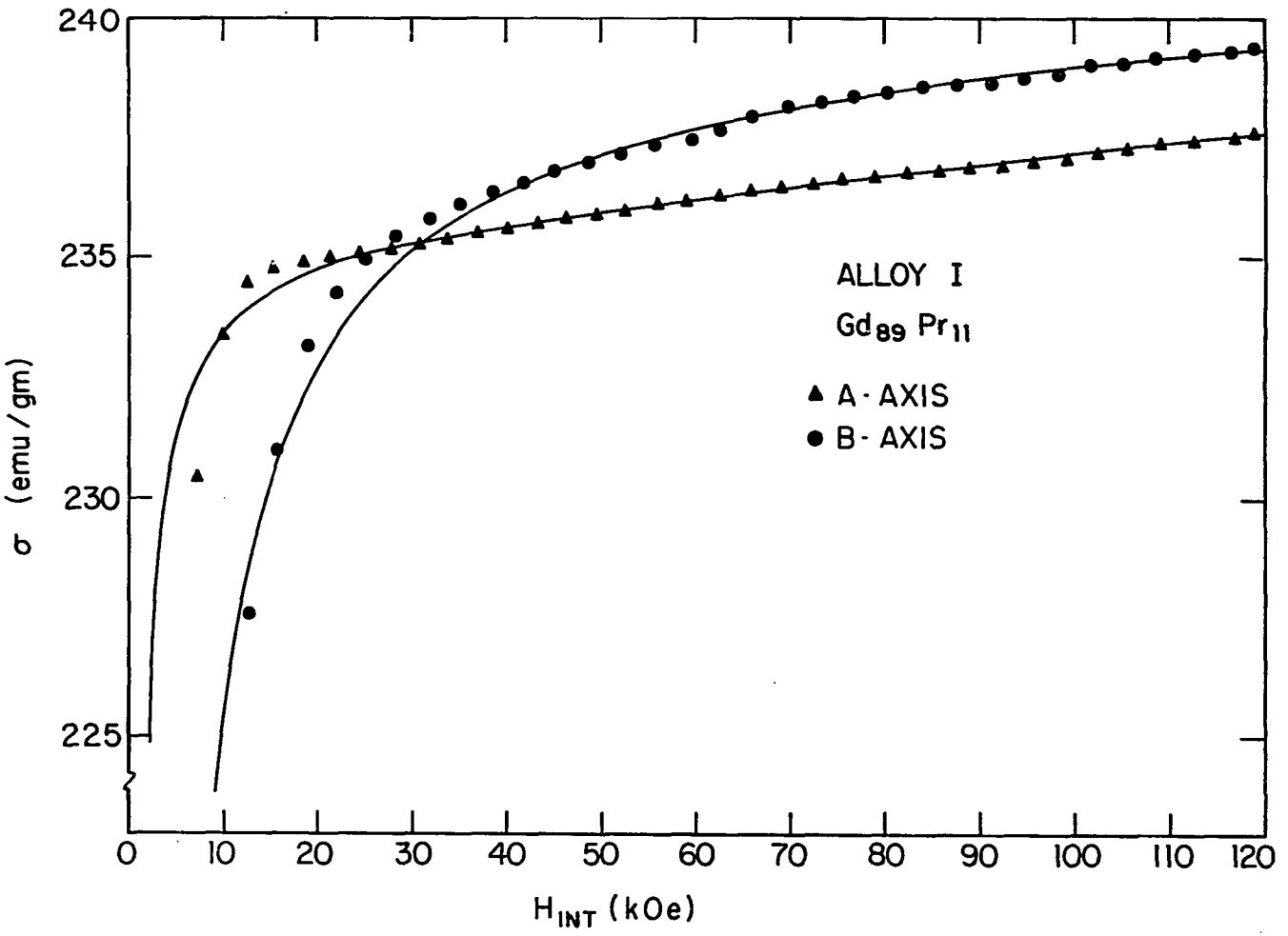

Figure 10. Isothermal magnetization of alloy I of $Gd_{89}Pr_{11}$ as a function of internal field. The solid curves represent a fit of the data to Eq. 40

For the a-axis sample

$$\sigma_0 = 235.4 \pm 0.7 \text{ emu gm}^{-1}$$

$$\chi = (2.0 \pm 1.4) \times 10^{-2} \text{ emu gm}^{-1} \text{ kOe}^{-1}$$

$$\alpha = -21 \pm 14 \text{ emu gm}^{-1} \text{ kOe.}$$

For the b-axis sample

$$\sigma_0 = 239.6 \pm 0.7 \text{ emu gm}^{-1}$$

$$\chi = (8.0 \pm 5.6) \times 10^{-2} \text{ emu gm}^{-1} \text{ kOe}^{-1}$$

$$\alpha = -140 \pm 6 \text{ emu gm}^{-1} \text{ kOe.}$$

These values of the saturation magnetization correspond to values of 6.55 ± 0.03 μ_B/atom and 6.67 ± 0.03 μ_B/atom for the average moment per atom for the a- and b-axis samples, respectively.

The possibility that this anomalous behavior was the result of differences in concentration was considered. In order to account for the observed differences in magnetization, the two samples would have to differ by about one percent in gadolinium concentration. This difference should manifest itself in the Curie temperatures of the two samples. Accordingly, isofield magnetization measurements at temperatures ranging from 240 K to 290 K were performed in an applied field of 334 Oe using a vibrating sample magnetometer described in detail by Burgardt (34). The results of these measurements are shown in Figure 11. As can be seen from the figure, the data points for the b-axis sample fall directly on top of the data points for the a-axis sample throughout the ferromagnetic transition. A Curie temperature of 254.4 ± 0.5 K is obtained from the inflection point for both samples. Assuming a linear relationship between the depression of the Curie temperature from that of pure

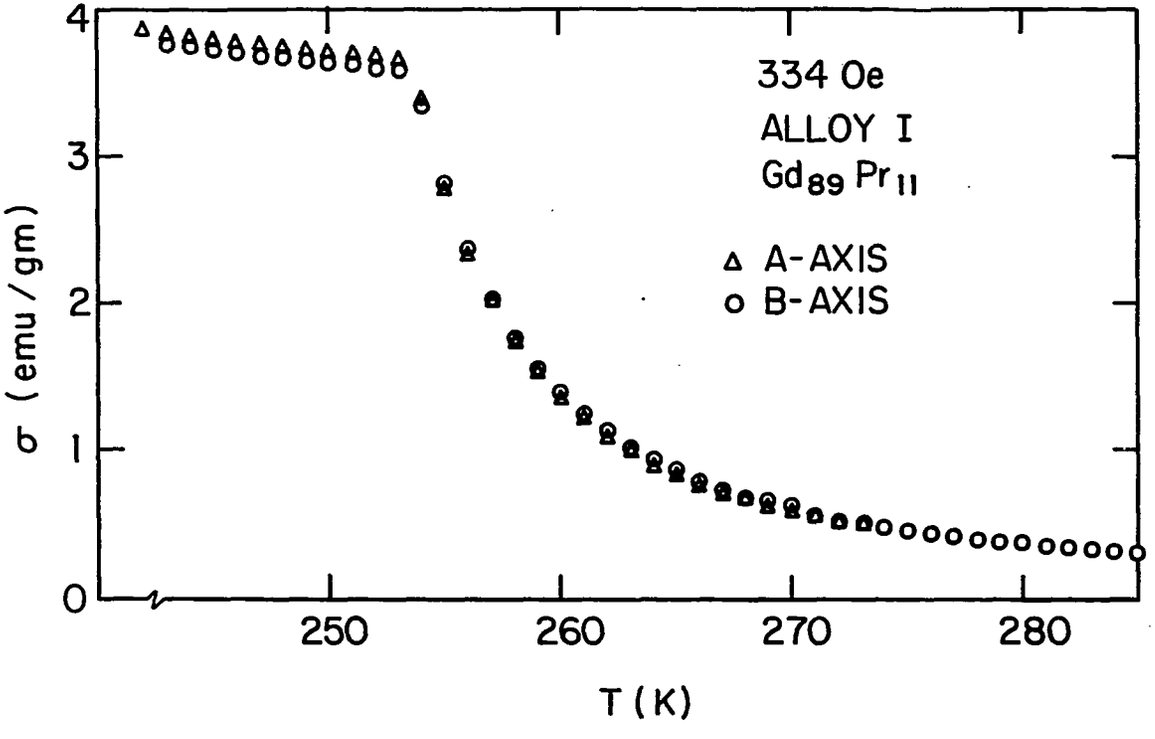

Figure 11. Isofield magnetization of alloy I of $Gd_{89}Pr_{11}$ as a function of temperature

gadolinium with praseodymium concentration, a difference of 5 K would be expected for two samples differing in concentration by one percent. Thus, it is seen that concentration differences can not account for the anomalous behavior in the magnetization.

At this point, metallographic studies were performed on both samples. The results of these studies indicated that, except for minor surface defects, both samples were single crystals and single phase. It has been previously discussed in the section on sample preparation that the preparation of alloy I was somewhat peculiar. Operating under the assumption that some aspect of this abnormal preparation process was responsible for the anomalies in the magnetization curves, two new samples of identical composition, known as alloy II, were prepared by more normal procedures. Results of isothermal magnetization measurements on these two samples are shown in Figure 12. As can be seen from the figure, the anomalous behavior of the alloy I samples is not observed in the alloy II samples. The solid curves represent fits of the data to Eq. 40. The results of these fits are:

For the a-axis sample

$$\sigma_0 = 235.6 \pm 0.7 \text{ emu gm}^{-1}$$

$$\chi = (1.7 \pm 1.2) \times 10^{-3} \text{ emu gm}^{-1} \text{ kOe}^{-1}$$

$$\alpha = -18.3 \pm 3.4 \text{ emu gm}^{-1} \text{ kOe}.$$

For the b-axis sample

$$\sigma_0 = 235.9 \pm 0.7 \text{ emu gm}^{-1}$$

$$\chi = (4.0 \pm 2.8) \times 10^{-3} \text{ emu gm}^{-1} \text{ kOe}^{-1}$$

$$\alpha = -66 \pm 12 \text{ emu gm}^{-1} \text{ kOe}.$$

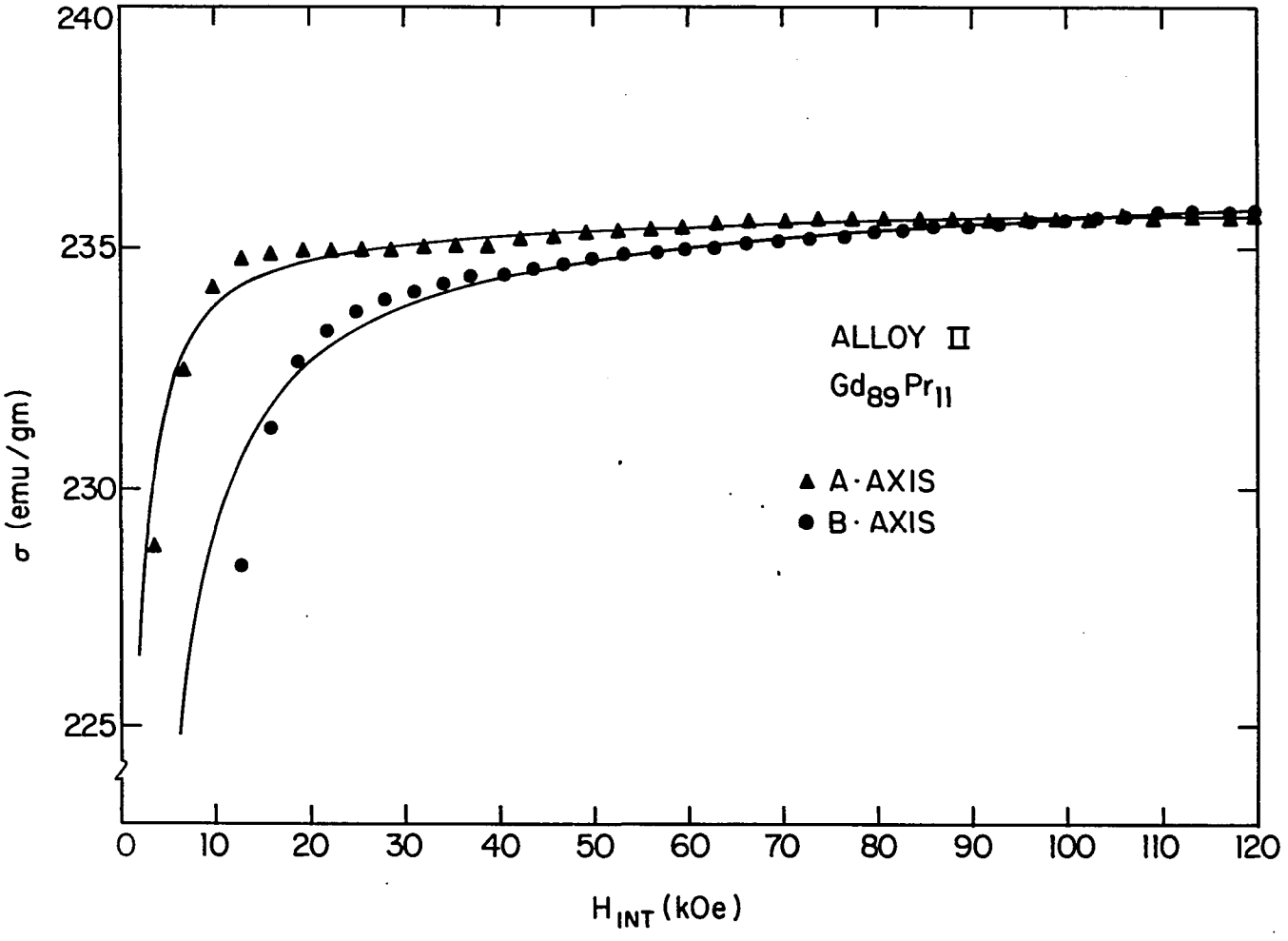

Figure 12. Isothermal magnetization of alloy II of $Gd_{89}Pr_{11}$ as a function of internal field. The solid curves represent a fit of the data to Eq. 40

These values of the saturation magnetization correspond to values of $6.56 \pm 0.03\ \mu_B$/atom and $6.57 \pm 0.03\ \mu_B$/atom for the average moment per atom of the a- and b-axis samples, respectively. As the figure shows, there is some anisotropy between the two directions, with the a-axis being the easier direction. Thus, the average saturation moment per atom for an alloy of 11.0 atomic percent praseodymium in gadolinium is taken to be $6.56 \pm 0.03\ \mu_B$/atom.

D. 8.3% Ce in Gd

Results of isothermal magnetization measurements on a- and b-axis single crystals of an alloy of 8.3 atomic percent cerium in gadolinium performed at a temperature of 4.2 K are shown in Figure 13. An adequate fit to Eq. 40 could not be made with these data. Thus, it was necessary to go to the next order in $1/H_{int}$ to obtain an adequate fit. The solid curves in Figure 13 represent a fit of the data to the expression

$$\sigma = \sigma_0 + \chi H_{int} + \alpha H_{int}^{-1} + \beta H_{int}^{-2} . \qquad (45)$$

The results of a fit of the data to Eq. 45 are:

For the a-axis sample

$$\sigma_0 = 245.0 \pm 2.0 \text{ emu gm}^{-1}$$

$$\chi = (3.5 \pm 2.5) \times 10^{-2} \text{ emu gm}^{-1} \text{ kOe}^{-1}$$

$$\alpha = (7.0 \pm 1.3) \times 10^{2} \text{ emu gm}^{-1} \text{ kOe}$$

$$\beta = (-2.31 \pm 0.15) \times 10^{4} \text{ emu gm}^{-1} \text{ kOe}^{2}.$$

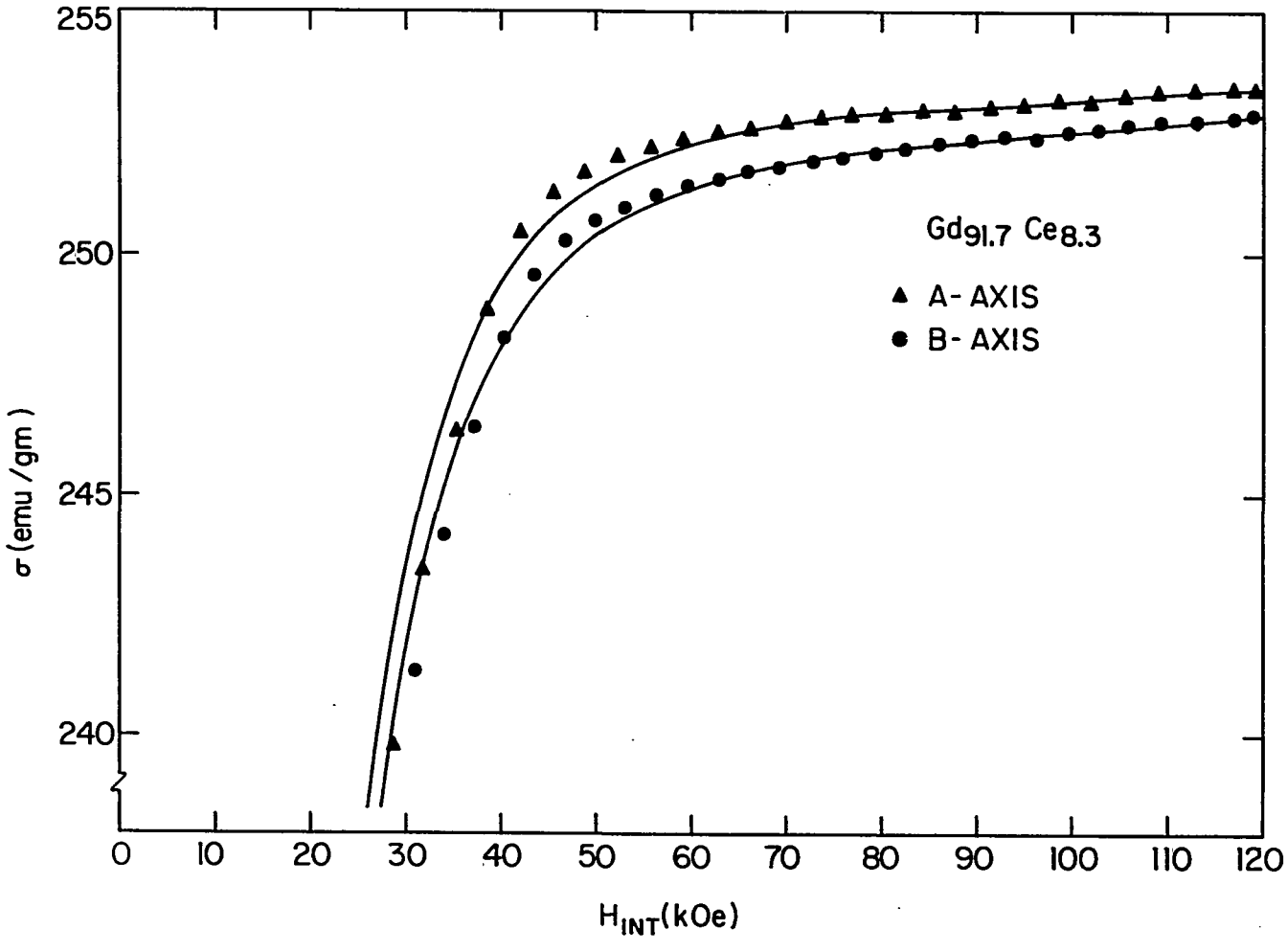

Figure 13. Isothermal magnetization of $Gd_{91.7}Ce_{8.3}$ as a function of internal field. The curves represent a fit of the data to Eq. 45

For the b-axis sample

$$\sigma_0 = 244.1 \pm \text{emu gm}^{-1}$$

$$\chi = (3.9 \pm 2.7) \times 10^{-2} \text{ emu gm}^{-1} \text{ kOe}^{-1}$$

$$\alpha = (7.0 \pm 1.3) \times 10^{2} \text{ emu gm}^{-1} \text{ kOe}$$

$$\beta = (-2.39 \pm 0.10) \times 10^{4} \text{ emu gm}^{-1} \text{ kOe}^{2}.$$

These values of the saturation magnetization correspond to values of 6.84 ± 0.06 μ_B/atom and 6.81 ± 0.06 μ_B/atom for the average moment per atom of the a- and b-axis samples, respectively. As the figure shows, there is a slight anisotropy between the two directions, with the a-axis direction being slightly easier. Thus, the average saturation moment per atom for an alloy of 8.3 atomic percent cerium in gadolinium is taken to be 6.84 ± 0.06 μ_B/atom.

V. DISCUSSION

In order to understand the magnetization results, it is necessary to develop a model describing the magnetization of an alloy of a light rare earth with gadolinium. Two separate models will be discussed. In the first case, spin-orbit coupling is assumed to be the dominant interaction, and thus the Hamiltonian of Eq. 26 is assumed to hold. This case will be known as the J-J coupling case. The second case assumes that the exchange interaction dominates, and thus the Hamiltonian of Eq. 19 holds. This case will be known as the S-S coupling case. For both cases, a simple vector picture will be used. An expression predicting the magnetization due to the ionic moments will be developed for each case. Next, the contribution to the magnetization due to the conduction electron polarization will be considered.

For the J-J coupling case, the ground state will be characterized by either a parallel or an antiparallel alignment of the two magnetic moments. The J value of the light rare earth ion is still a good quantum number. Thus, the net ionic contribution to the magnetization, M_i, is simply the sum or difference of the moments carried by the individual ions. That is,

$$M_i = (c_{Gd} g_{Gd} S_{Gd} \pm c_{lre} g_{lre} J_{lre}) \mu_B \tag{46}$$

where c_{lre} is the concentration of light rare ions, g_{lre} is the g value of the light rare earth ion, J_{lre} is the total angular momentum of the light rare earth ion, c_{Gd} is the concentration of gadolinium ions, g_{Gd} is the g factor for gadolinium, and S_{Gd} is the spin of a gadolinium ion.

For the S-S coupling case, the picture is not as simple. The dominance of the exchange term is interpreted to mean that the spin vectors of the gadolinium and light rare earth ions will be forced into either a parallel or an antiparallel alignment. Due to the spin orbit interaction, there will be a finite angle, α_{SJ}, between the spin vector and the total momentum vector in the light rare earth ions. Because of the constraint of parallel spin alignment, the simple vector picture indicates that the J vector of the light rare earth ion will precess about the common spin direction. This consideration is not important in the gadolinium ions since they are characterized by a pure spin moment. Thus, the net ionic contribution to the magnetization is

$$M_i = (c_{Gd} g_{Gd} S_{Gd} \pm c_{lre} g_{lre} J_{lre} \cos \alpha_{SJ}) \mu_B \ . \tag{47}$$

The problem is now reduced to finding the value of α_{SJ}. For the purposes of this simple model, the value of α_{SJ} is taken to be that of a free light rare earth ion in the absence of the exchange interaction. Such an ion is characterized by the state $|S\ L\ J\ M_J\rangle$, where S, L, and J are determined by the Hund rules. In a free ion, the spin-orbit interaction will cause the S vector to precess about the J vector. Thus, the magnitude of the expectation value of the S vector is given by

$$\langle \bar{S} \rangle^2 = \langle \bar{S}^2 \rangle \cos^2 \alpha_{SJ} = S(S + 1) \cos^2 \alpha_{SJ} \tag{48}$$

From the projection theorem, which is a direct result of the Wigner-Eckart theorem,

$$\langle \bar{S} \rangle = \frac{\langle S\ L\ J\ m | \bar{S} \cdot \bar{J} | S\ L\ J\ m \rangle}{J(J + 1)} \langle \bar{J} \rangle \ . \tag{49}$$

From the relation $\bar{J} = \bar{L} + \bar{S}$, it can be shown that

$$\bar{S} \cdot \bar{J} = \frac{1}{2} (\bar{J}^2 + \bar{S}^2 - \bar{L}^2) . \tag{50}$$

Combining Eqs. 49 and 50 yields

$$\langle \bar{S} \rangle = \frac{1}{2} \frac{[J(J + 1) + S(S + 1) - L(L + 1]}{J(J + 1)}$$

$$= (g - 1) \langle \bar{J} \rangle . \tag{51}$$

Thus, it is seen that

$$\langle \bar{S} \rangle^2 = (g - 1)^2 \langle \bar{J} \rangle^2 = (g - 1)^2 J(J + 1) \tag{52}$$

Combining Eqs. 48 and 52 yields

$$\cos^2 \alpha_{SJ} = (g - 1)^2 \frac{J(J + 1)}{S(S + 1)} . \tag{53}$$

For the light rare earths, which have a less than half filled 4f shell, $J = L - S$. Thus,

$$\cos^2 \alpha_{SJ} = \frac{SJ}{(J + 1)(S + 1)} . \tag{54}$$

Thus, the approximate value of α_{SJ} has been determined.

The next problem is to determine the contribution to the magnetization due to the conduction electron polarization for each case. From Eq. 23, it is seen that the conduction electron contribution to the magnetization is proportional to the average spin. Thus, the approximation is made that M_e, the contribution to the magnetization due to the conduction electrons, is given by

$$M_e = M_e(Gd) \langle S \rangle / S_{Gd} \tag{55}$$

where $M_e(Gd)$ is the conduction electron polarization for the pure host gadolinium, S_{Gd} is the spin of gadolinium, and $\langle S \rangle$ is the average spin

per ion of the alloy. It is noted that it is inherent in this approximation that the matrix element of Eq. 23 is constant over the rare earth series. The problem now becomes that of determining the value of <S> for each case.

For the J-J coupling case, the spin of the light rare earth ion precesses about the common J direction. Thus, in calculating the average spin, it is appropriate to project the S vector onto the J vector. Again, this is not a problem in the gadolinium ion since gadolinium is characterized by a pure spin moment. Thus, the average spin in the J-J coupling case is given by

$$S = c_{Gd}S_{Gd} \mp c_{lre}S_{lre} \cos \alpha_{SJ} \tag{56}$$

where S_{lre} is the spin of the light rare earth ion, and $\cos \alpha_{SJ}$ is given by Eq. 54. Since the spin is in the opposite direction of the total angular momentum in the light rare earths, the plus sign should be used if the minus sign is used in Eq. 46. Correspondingly, the minus sign is used in Eq. 56 if the plus sign is used in Eq. 46.

Thus, it has been seen that, under a simple vector model, the magnetization of an alloy of a light rare earth with gadolinium has been determined for both the J-J and S-S coupling cases. For the J-J coupling case, the predicted moment is

$$\mu_{sat}(J\text{-}J) = (c_{Gd}g_{Gd}S_{Gd} \pm c_{lre}g_{lre}J_{lre})\mu_B + \frac{M_e(Gd)}{S_{Gd}} (c_{Gd}S_{Gd} \mp c_{lre}S_{lre} \cos \alpha_{SJ}) . \tag{57}$$

For the S-S coupling case, the approximate moment is given by

$$\mu_{sat}(S\text{-}S) = (c_{Gd}g_{Gd} \pm c_{1re}g_{1re}J_{1re}\cos\alpha)\mu_B + \frac{M_e(Gd)}{S_{Gd}}(c_{Gd}S_{Gd} \mp c_{1re}S_{1re}) . \quad (58)$$

The next task is to calculate the predicted values of the saturation magnetization for each of the alloys on which measurements were performed. Results of these calculations for both the J-J and S-S coupling cases will be presented.

For an alloy of 14.5 atomic percent neodymium in gadolinium, the results are as follows:

For the J-J coupling case with J vectors antiparallel

$$\mu_{sat} = 6.12 \pm 0.03\ \mu_B/\text{atom};$$

for the J-J coupling case with J vectors parallel

$$\mu_{sat} = 7.01 \pm 0.03\ \mu_B/\text{atom};$$

for the S-S coupling case with spin vectors parallel

$$\mu_{sat} = 6.28 \pm 0.03\ \mu_B/\text{atom};\ \text{and}$$

for S-S coupling with spin vectors antiparallel

$$\mu_{sat} = 6.86 \pm 0.03\ \mu_B/\text{atom}.$$

The errors in these predictions are due to errors in the measured values of the conduction electron polarization in Gd I.

For an alloy of 11.0 atomic percent praseodymium in gadolinium, the results are as follows:

For the J-J coupling case with J vectors antiparallel

$$\mu_{sat} = 6.52 \pm 0.04\ \mu_B/\text{atom};$$

for the J-J coupling case with J vectors parallel

$$\mu_{sat} = 7.19 \pm 0.04\ \mu_B/\text{atom};$$

for the S-S coupling case with S vectors parallel

$$\mu_{sat} = 6.65 \pm 0.04\ \mu_B/\text{atom};\ \text{and}$$

for the S-S coupling case with S vectors antiparallel

$$\mu_{sat} = 7.05 \pm 0.04\ \mu_B/\text{atom}.$$

For an alloy of 8.3 atomic percent cerium in gadolinium, the results are as follows:

For the J-J coupling case with J vectors antiparallel

$$\mu_{sat} = 6.89 \pm 0.04\ \mu_B/\text{atom};$$

for the J-J coupling case with J vectors parallel

$$\mu_{sat} = 7.23 \pm 0.04\ \mu_B/\text{atom};$$

for the S-S coupling case with S vectors parallel

$$\mu_{sat} = 6.98 \pm 0.04\ \mu_B/\text{atom};\ \text{and}$$

for the S-S coupling case with S vectors antiparallel

$$\mu_{sat} = 7.14 \pm 0.04\ \mu_B/\text{atom}.$$

Again, the errors in the predictions for these two alloys are a result of errors in the measurement of the conduction electron polarization in Gd II.

The measured value of the saturation magnetization for an alloy of 14.5 atomic percent neodymium in gadolinium was found to be

6.08 ± 0.03 μ_B/atom. Within error, this value coincides with the predicted value of 6.12 ± 0.03 μ_B/atom for the J-J coupling case, with the J vectors in an antiparallel alignment. The next closest prediction to the observed value is 6.28 ± 0.03 μ_B/atom, predicted for the S-S coupling case, with spin vectors in parallel alignment. This value does not lie within error of the measured value. The measured value of the saturation magnetization for an alloy of 11.0 atomic percent praseodymium in gadolinium was found to be 6.56 ± 0.03 μ_B/atom. Within error, this value coincides with the predicted value of 6.52 ± 0.04 μ_B/atom for the J-J coupling case, with the J vectors in an antiparallel alignment. The next closest prediction to the observed value is 6.65 ± 0.04 μ_B/atom, predicted for the S-S coupling case, with spin vectors in parallel alignment. This value does not lie within error of the measured value. The measured value of the saturation magnetization for an alloy of 8.3 atomic percent cerium in gadolinium was found to be 6.84 ± 0.06 μ_B/atom. Within error, this value coincides with the predicted value of 6.89 ± 0.04 μ_B/atom for the J-J coupling case, with the J vectors in an antiparallel alignment. Again, the next closest prediction to the observed value is 6.98 ± 0.04 μ_B/atom, predicted for the S-S coupling case, with spin vectors in parallel alignment. This value does not lie within error of the measured value. All of the preceding results are shown collectively in Figure 14. The solid circles in the Figure represent the values of the saturation magnetization predicted for the various cases by the vector model. The arrows represent the relative orientations of the spin vectors for the S-S cases and the J vectors for the J-J

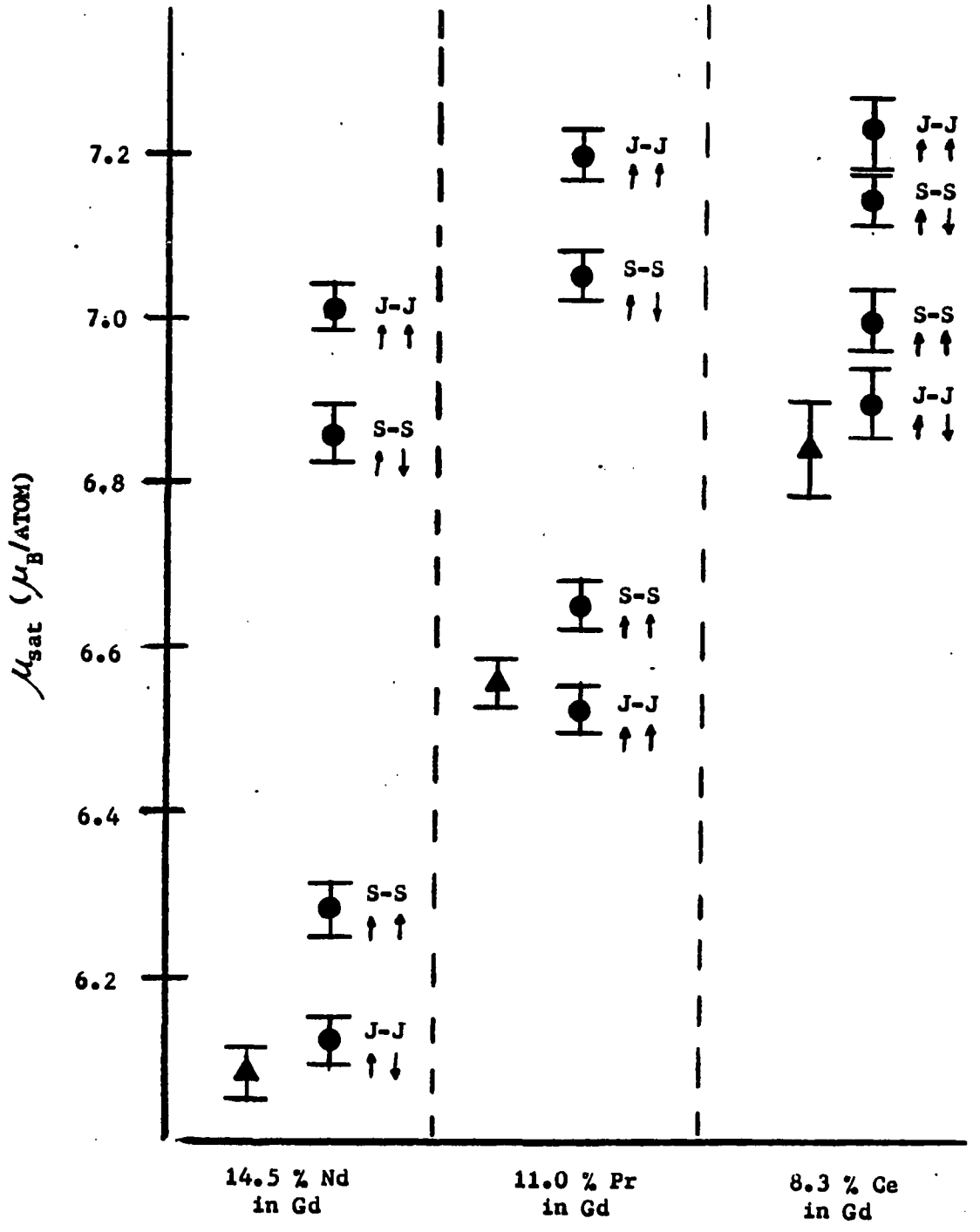

Figure 14. The solid circles represent the predictions of the simple vector model for the saturation magnetization for the various cases. The arrows represent the relative orientations of the vectors. The solid triangles represent the measured value of the saturation magnetization for each of the alloys shown

cases. The solid triangles represent the measured values, and are shown for comparison with the values predicted for the various cases.

Thus, it has been seen that a simple vector model based upon the assumption of an antiparallel J-J coupling interaction provide adequate predictions of the saturation magnetizations of the three alloys examined in this study. Furthermore, it has been seen that a model based upon an S-S coupling interaction fails to account for the observed saturation magnetizations of these alloys. These results tend to support the suggestion of de Gennes that due to strong spin-orbit coupling, the spin momentum should be replaced by its projection onto the total angular momentum in the interaction Hamiltonian.

VI. ACKNOWLEDGEMENTS

I would like to thank Dr. Sam Legvold, my major advisor. Many of the ideas which he imparted will remain with me for the rest of my life. He is unquestionably one of the finest educators whom I have ever had the occasion to know.

I would also like to acknowledge the support, both technical and moral, of the following people: Dr. Paul Burgardt, who introduced me to some of the harsher realities of graduate life; Joel Hendrickson, who was always willing to listen to my ideas; Dr. Michael Padgett, who truly understood my frustrations; Mr. B. J. Beaudry, an outstanding metallurgist, who produced sample after sample after sample; Mr. Jerry Ostenson, who was always willing to help puzzle over belligerent apparatus; Mr. Ed Sexauer and Mr. Dick Brown, who introduced me to the fine art of precision machine work. The friendship and advice of these people have been a great aid to me throughout my graduate career.

Special thanks are in order for the immediate members of my family. They have constantly stood by me with encouragement through all the long years.

Finally, I would like to express my gratitude to my future wife, Marge Richardson. Without her unending faith in my abilities, I doubt that this work would have ever attained its present level of completion.

VII. LITERATURE CITED

1. S. Legvold, Ferromagnetic Materials, edited by E. P. Wohlfarth (North-Holland, Amsterdam, 1980), Vol. 1, Chap. 3.

2. G. S. Anderson and S. Legvold, Phys. Rev. Lett. 1, 322 (1958).

3. R. Brout and H. Suhl, Phys. Rev. Lett. 2, 387 (1959).

4. S. Legvold, Phys. Rev. B 3, 1640 (1971).

5. A. R. Mackintosh and F. A. Smidt, Jr., Phys. Lett. 2, 107 (1962).

6. S. Legvold, J. H. Queen, B. J. Beaudry, and B. N. Harmon, Journal of Magnetism and Magnetic Materials 15-18, 1221 (1979).

7. P. Weiss, J. de Physique, Ser. 4, 6, 661 (1907).

8. W. Heisenberg, Z. Physik 49, 619 (1928).

9. M. A. Ruderman and C. Kittel, Phys. Rev. 96, 99 (1954).

10. T. Kasuya, Progr. Theor. Phys. (Kyoto) 16, 45 (1956).

11. K. Yosida, Phys. Rev. 106, 893 (1957).

12. T. Kasuya, Magnetism, edited by G. T. Rado and H. Suhl (Academic Press, New York, 1966), Vol. IIB, p. 215.

13. S. H. Liu, Phys. Rev. 123, 470 (1961).

14. K. Yosida, Phys. Rev. 107, 396 (1957).

15. P. G. de Gennes, C. R. Acad. Sci. (Paris) 247, 1836 (1958).

16. T. Kasuya, Progr. Theoret. Phys. (Kyoto) 22, 227 (1958).

17. R. J. Elliott, Magnetic Properties of Rare Earth Metals, edited by R. J. Elliott (Plenum Press, New York, 1972), Chap. 1.

18. G. H. Dieke, Spectra and Energy Levels of Rare Earth Ions in Crystals, (Wiley, New York, 1961).

19. S. Foner, Rev. Sci. Instr. 30, 548 (1959).

20. D. B. Richards, L. R. Edwards, C. M. Cornforth, and S. Legvold, Rev. Sci. Instr. 41, 647 (1970).

21. L. W. Roeland, G. J. Cock, F. A. Muller, A. C. Moleman, K. A. McEwen, R. G. Jordan,a nd D. W. Jones, J. Phys. F 5, L233 (1975).

22. H. Danan, A. Herr, and A. J. P. Meyer, J. Appl. Phys. 39, 669 (1968).

23. P. Weiss, J. de Physique, Ser. 4, 9, 373 (1910).

24. R. M. Bozorth, Ferromagnetism, (D. Van Nostrand, New York, 1951).

25. P. R. Bevington, Data Reduction and Error Analysis for the Physical Sciences, (McGraw-Hill, New York, 1969), Chap. 8, p. 140.

26. F. Bloch, Z. Physik 61, 206 (1930).

27. E. C. Stoner, Reports on Progress in Physics 11, 43 (1948).

28. H. E. Nigh, S. Legvold, and F. H. Spedding, Phys. Rev. 132, 1092 (1963).

29. G. Will, R. Nathans, and H. A. Alperin, J. Appl. Phys. 35, 1045 (1964).

30. J. W. Cable, and E. O. Wollan, Phys. Rev. 165, 733 (1968).

31. H. W. White, B. J. Beaudry, P. Burgardt, S. Legvold, and B. N. Harmon, A. I. P. Conference Proceedings 29, 329 (1975).

32. H. Fujimori, K. Goto, and D. E. G. Williams, J. Phys. F 4, 2152 (1974).

33. S. Legvold, P. Burgardt, and B. J. Beaudry, Crystal Field Effects in Metals and Alloys, edited by A. Furrer (Plenum Publishing Corporation, New York, 1977), p. 340.

34. P. Burgardt, Ph.D. Thesis, Iowa State University Library, 1976 (unpublished).